Available online at www.sciencedirect.com
ScienceDirect
ELSEVIER
Palaeogeography, Palaeoclimatology, Palaeoecology 244 (2007) 11–33
PALAEO
www.elsevier.com/locate/palaeo

Triassic–Jurassic boundary events inferred from integrated stratigraphy of the Csővár section, Hungary

József Pálfy [a,*], Attila Demény [b], János Haas [c], Elizabeth S. Carter [d], Ágnes Görög [e], Dóra Halász [f], Anna Oravecz-Scheffer [g], Magdolna Hetényi [h], Emő Márton [f], Michael J. Orchard [i], Péter Ozsvárt [a], István Vető [j], Norbert Zajzon [k]

[a] *Research Group for Palaeontology, Hungarian Academy of Sciences-Hungarian Natural History Museum, POB 137, Budapest, H-1431, Hungary*
[b] *Institute for Geochemical Research, Hungarian Academy of Sciences, Budaörsi út 45, Budapest, H-1112, Hungary*
[c] *Research Group for Geology, Hungarian Academy of Sciences-Eötvös University, Pázmány P. sétány 1/c, Budapest, H-1117, Hungary*
[d] *Department of Geology, Portland State University, P.O. Box 751, Portland, OR 97207-0751, USA*
[e] *Department of Palaeontology, Eötvös University, Pázmány P. sétány 1/c, Budapest, H-1117, Hungary*
[f] *Palaeomagnetic Laboratory, Eötvös Loránd Geophysical Institute of Hungary, Kolumbusz u. 17-23, Budapest, H-1145, Hungary*
[g] *Hűvösvölgyi út 74, Budapest, H-1021, Hungary*
[h] *Department of Mineralogy, Geochemistry and Petrology, University of Szeged, Egyetem u. 2-6, Szeged, H-6722, Hungary*
[i] *Geological Survey of Canada, 101-605 Robson Street, Vancouver, BC, Canada V6B 5J3*
[j] *Geological Institute of Hungary, Stefánia út 14, Budapest, H-1143, Hungary*
[k] *Department of Mineralogy and Petrology, University of Miskolc, Miskolc-Egyetemváros, H-3515, Hungary*

Received 20 April 2005; accepted 20 June 2006

Abstract

Processes and causes of biotic and environmental change at the Triassic–Jurassic transition remain controversial, partly because of a scarcity of Triassic–Jurassic boundary sections studied in detail. Continuous marine strata spanning the boundary are exposed at Csővár, Hungary, where new integrated stratigraphic data were obtained from multidisciplinary investigations to help reconstruct the end-Triassic and Early Jurassic events. Boundary strata are predominantly slope to basinal carbonates deposited in a periplatform basin. The position of the system boundary is constrained by radiolarian, foraminiferan, conodont and ammonoid biostratigraphy. Pronounced radiolarian turnover is observed between assemblages assigned to the Late Rhaetian *Globolaxtorum tozeri* zone and the Early Hettangian *Canoptum merum* zone. Benthic foraminifera suffered lesser extinction. Successive conodont faunas of the latest Rhaetian *Misikella posthersteini* and *Misikella ultima* zones record a marked drop in diversity and abundance but sporadic survivors persist into the earliest Hettangian. The extinction is also recorded in a reduction of biogenic components in carbonates. Decline of benthic and planktic biota is followed by a negative $\delta^{13}C_{carb}$ excursion of up to −6‰ that is composed of short-term fluctuations revealed by dense sampling. Carbon and oxygen isotope ratios are positively correlated in the lower part of the section and appear to reflect primary variations. Drivers of the stable isotope trends are interpreted as warming in excess of +10 °C and concomitant episodic, short-term perturbations of the global carbon cycle, possibly due to methane release

* Corresponding author.
E-mail address: palfy@nhmus.hu (J. Pálfy).

0031-0182/$ - see front matter
doi:10.1016/j.palaeo.2006.06.021

from gas–hydrate dissociation induced by rapid climatic events. The main biotic and isotopic events occurred within a single sedimentary cycle but sea-level does not appear to have exerted a critical influence on these changes. The Triassic–Jurassic boundary crisis appears a short but not instantaneous event.

Keywords: Triassic–Jurassic boundary; Integrated stratigraphy; Extinction; Carbon isotope; Sea-level change

1. Introduction

The Triassic–Jurassic (T–J) boundary is marked by major biotic extinction (Sepkoski, 1996) and environmental perturbations (Tanner et al., 2004). Previously, the least studied of the "Big Five" extinction events (Hallam, 1990), this boundary has received considerable attention recently. Significant advances have been made in understanding the evolutionary turnover of affected fossil groups (see summary in Hallam, 2002), and the geochemical history of marine and terrestrial environments (Pálfy et al., 2001; Hesselbo et al., 2002; Ward et al., 2004), improving correlation using various stratigraphic methods and establishing a more accurate time scale (Pálfy et al., 2000). The search for trigger mechanisms has focused on synchronous rare geological events, primarily the flood basalt volcanism of the Central Atlantic Magmatic Province (Marzoli et al., 1999; Pálfy, 2003; Marzoli et al., 2004) and a putative bolide impact (Olsen et al., 2002). Despite the recent progress, disagreement remains in many key questions about the magnitude and trajectory of changes, as well as the causes and mechanisms of T–J boundary events (Tanner et al., 2004).

Here we present new data from integrated studies of a marine T–J boundary section at Csővár, Hungary. Thin-bedded, cherty limestone of supposed Early Jurassic age was recognized in this area during geological reconnaissance already in the mid-19th century (Szabó, 1860). On the basis of more detailed work by Vadász (1910), the outcrops were then long regarded as entirely Late Triassic, Carnian in age. Finds of *Choristoceras* from the presently abandoned Pokol-völgy ("Hell Valley") quarry at Csővár suggested a younger age (Norian, according to Detre et al., 1988 or Rhaetian, according to Haas et al., 1997), and this was further supported by micropalaeontological data (Kozur and Mock, 1991). Radiolarians from cherty limestone near the top of Vár-hegy ("Castle Hill") at Csővár indicated that the uppermost exposed part of the Csővár Formation is Early Jurassic in age (Hettangian to Sinemurian) (Kozur, 1993). The presence of a T–J boundary section was proved by a preliminary biostratigraphic study of artificial trenches connecting the natural outcrops on the south slope of Vár-hegy (Pálfy and Dosztály, 2000). Conodont biostratigraphy provided further constraints on the T–J boundary, whereas facies and geochemical studies highlighted the significance of this section in preserving a continuous marine sedimentary record and established one of the first well-documented examples of a major negative $\delta^{13}C$ excursion across the T–J boundary (Pálfy et al., 2001). The lower part of the Csővár Formation at Pokol-völgy, exposed in the quarry and penetrated by a drill core, was the subject of an integrated stratigraphic and facies study (Haas et al., 1997). This demonstrated that the dominant calcareous turbidites and intercalated debris-flow layers represent slope, toe-of-slope and basinal depositional environments. Sedimentological investigations at the Vár-hegy section revealed that the T–J boundary transition shows similar facies characteristics to the quarry section and elucidated the history of sedimentary basin evolution (Haas and Tardy-Filácz, 2004). Detailed tectonic studies have resulted in better understanding of the post-Jurassic structural evolution of the Csővár block (Benkő and Fodor, 2002).

In this paper, we: (1) document the radiolarian, foraminiferan, conodont and ammonoid biostratigraphic framework in detail; (2) summarize the sea-level history inferred from facies studies; (3) report new geochemical analyses that establish a high-resolution stable isotope record across the principal T–J boundary anomaly and further extend the stable isotope record into the Hettangian; and (4) complement these data with results from organic geochemical, palaeomagnetic and micromineralogical studies. These results are used in discussing and testing different models and scenarios for the T–J boundary events.

2. Geologic setting

The fault-bounded Csővár block is located about 40 km NNW of Budapest, on the east side of the Danube River (Fig. 1). It represents the northeasternmost extremity of the Transdanubian Range unit of the Alcapa terrane (Kovács et al., 2000). According to current palaeogeographic reconstructions (Haas et al., 1995; Gawlick et al., 1999; Haas, 2002; Csontos and Vörös, 2004), in the Late Triassic, this area was located close to the distal margin of the Dachstein carbonate platform system and was segmented by intraplatform basins.

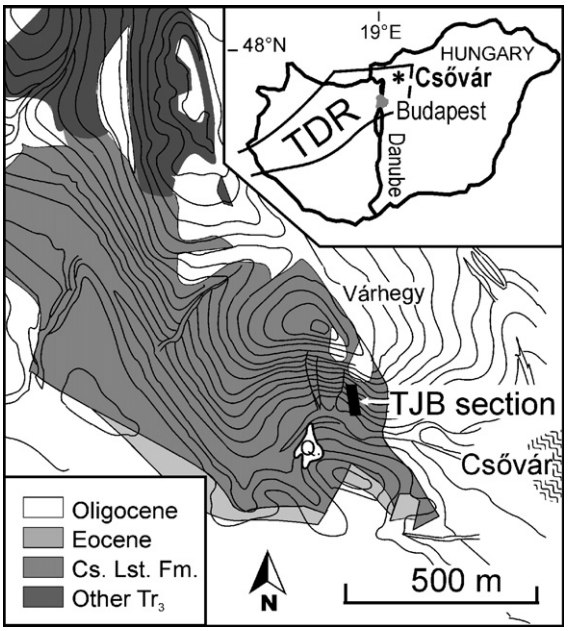

Fig. 1. Location index map of the Csővár section and simplified geology of the eastern part of Csővár block (after Benkő and Fodor, 2002). Coordinates for Bed 30 in the Late Triassic part of the measured section: 47°49′12.4″N, 19°18′32.5″E. Abbreviations: Q.—Pokol-völgy quarry (abandoned), Cs. Lst. Fm.—Csővár Limestone Formation, Tr_3—Late Triassic. Inset: location of Csővár within Hungary and the Transdanubian Range (TDR) tectonic unit.

In the northwestern part of the Csővár block, thick-bedded Late Carnian–Norian oncoidal facies of the Dachstein Limestone (Fig. 2) crops out. Southeastwards, in a zone about 1 km wide, coeval patch reef and proximal foreslope facies are preserved in the Nézsa Member of the Dachstein Formation (Benkő and Fodor, 2002). In the southeastern part of the block, thin-bedded, cherty dolostone and limestone (Csővár Limestone Formation) are exposed in the Pokol-völgy quarry and at other locations (Fig. 1). A drill core that was obtained from the yard of the quarry, penetrated the lower part of the Csővár Formation, representing rocks of Late Carnian–Early Rhaetian age (Haas et al., 1997). Cherty dolomite was encountered at the basal part of the Csővár Formation (Pokolvölgy Dolomite Member, Carnian in age). It is overlain by thin-bedded, laminated, locally cherty limestone of basinal, toe-of-slope and slope facies in a thickness of 500 m (Haas et al., 1997). The upper part of the Csővár Formation is exposed in the Pokol-völgy quarry (Haas et al., 1997) and in natural exposures and trenches on the steep southwestern slope of the Vár-hegy. The studied sections are located ca. 500 m west of the village of Csővár.

3. Facies characteristics and depositional cycles

The measured section of the Vár-hegy is shown in detail in Fig. 3, which illustrates the lithofacies types and the sequence stratigraphic depositional cycles (our terminology follows Vail et al., 1991; Schlager, 2005). A summary of the lithofacies types and their interpreted depositional setting is presented in Table 1. For a more detailed discussion, see Haas and Tardy-Filácz (2004). The Late Triassic stratigraphy known from the Pokol-völgy quarry and a drill core (Haas et al., 1997) is not presented here in detail but is considered in the interpretation. Based on the facies characteristics and the observed facies succession, the evolution of the depositional basin of the Csővár Formation is summarized as follows.

The inception of the Csővár Basin dates back to the Carnian, in connection with the opening of Neotethys. Extensional tectonics played an important role in the development of the basin and significantly influenced relative sea-level changes (Haas, 2002). The Csővár Formation was deposited in the Late Triassic on the foreslope of a carbonate platform and in the related intraplatform basin. Platform morphology and changes of water depth were controlled by the amount and composition of sediment exported to the slope and adjacent basin. Consequently, changes in the quantity and composition of bioclasts and lithoclasts in the gravity flow deposits can be used as an indicator of relative sea-level changes.

In the lower part of the Late Carnian–Norian succession (not discussed in detail in this study), basinal facies predominate, whereas distal toe-of-slope facies prevail higher up, suggesting that platform progradation occurred in the Late Norian (Haas, 2002). An abundance of continental elements in the flora in the basal layer of the Pokol-völgy quarry suggests a significant sea-level fall in the Early Rhaetian and subaerial exposure of large parts of the former platform. The sea-level fall led to increasing restriction of the intraplatform basin and establishment of oxygen-depleted bottom waters.

Above this basal layer, the facies characteristics suggest a long-term deepening trend in the Early Rhaetian to Early Hettangian interval. The lower part of the quarry section, representing the higher part of the Early Rhaetian succession, is characterized by the predominance of proximal turbidites with the intercalation of a single, 1-m-thick debrite. In the carbonate turbidite layers, crinoid fragments prevail and foraminifera of inner platform origin are missing. The abundance in some layers of sporomorphs of continental plants is remarkable (Haas et al., 1997). These observations suggest that a large part

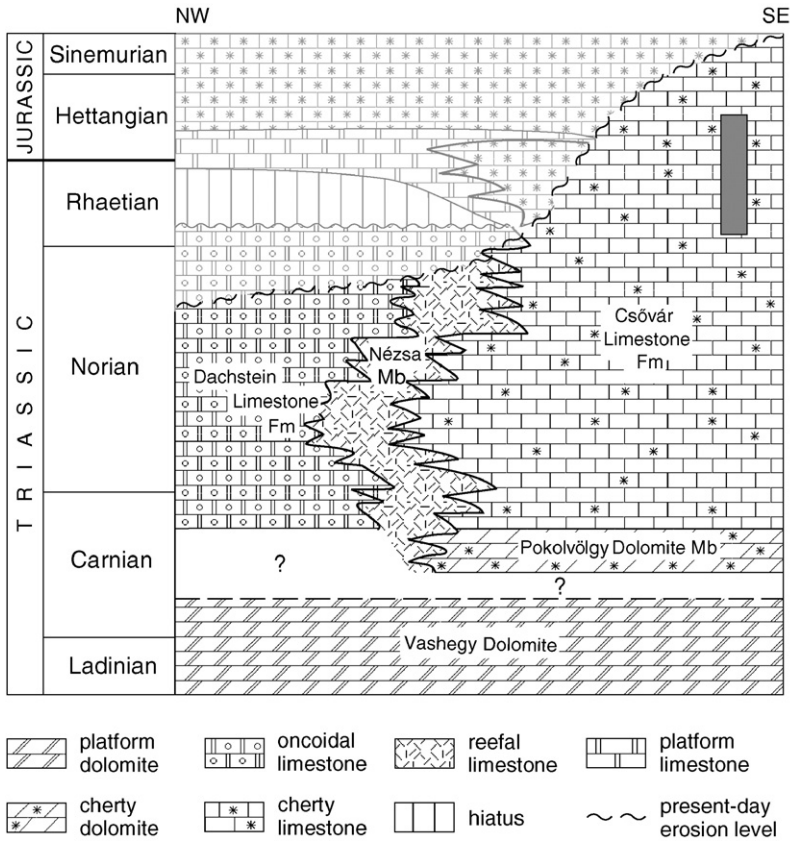

Fig. 2. Late Triassic to Early Jurassic stratigraphic model of the Csővár block along a NW–SE transect (after Haas and Tardy-Filácz, 2004). Pale pattern denotes missing parts of units removed by erosion. Position of the studied section marked by grey box. Width of depicted area is ca. 10 km.

of the neighbouring platform remained emergent in Early Rhaetian, and that a crinoid-dominated carbonate factory flourished on the slopes and supplied the carbonate turbidites. The debrite reflects instability of the slope for a relatively short period, probably due to falling relative sea-level (cf. Spence and Tucker, 1997) and it marks the base of a fourth-order cycle.

The Late Rhaetian to Early Hettangian history is interpreted from the lowermost part of the Vár-hegy section (Fig. 4). Superimposed upon the long-term (second-order) deepening upward trend, a metre-scale cyclicity is deciphered from the alternation of turbiditic and pure basinal facies. This cyclicity is more pronounced in the lower part of the Vár-hegy section where medium-grained turbidites are present, and is more vaguely defined or absent in the upper part (Fig. 3) where calcisiltite-calcilutite laminites (probably very distal turbidites) and typical basinal facies prevail.

The first fourth-order cycle in the Vár-hegy section (Beds 1–15, Figs. 3 and 4) begins with proximal and distal turbidites that grade upward into radiolarian basinal facies. This trend is interpreted to reflect retrogradation of the platform due to relative sea-level rise. Bed 16 contains large, redeposited bioclasts of platform origin, and is considered as the basal layer of the next cycle (Beds 16–29), which is mainly composed of laminated very distal turbidite facies. This interval is overlain by a distinctive layer (Bed 30) that contains small lithoclasts of cemented fragments of crinoids and a large number of shallow-marine skeletal elements in a pelagic wackestone matrix. Coarse-grained detritus of corals and molluscs occur in the topmost part of the bed. This bed is interpreted as a lowstand (fourth-order?) deposit. The appearance of a relatively large amount of sand to silt-size terrigenous siliciclasts in this bed is also interpreted to reflect low sea-level.

Above Bed 30, the appearance of the laminitic lithofacies (Beds 31–47) and radiolarian wackestone (Beds 48–51) clearly indicates a transgressive trend. These beds are overlain by a thin lithoclastic and bioclastic proximal turbidite layer (Bed 52), which may be considered as the base of the next sedimentary cycle, but

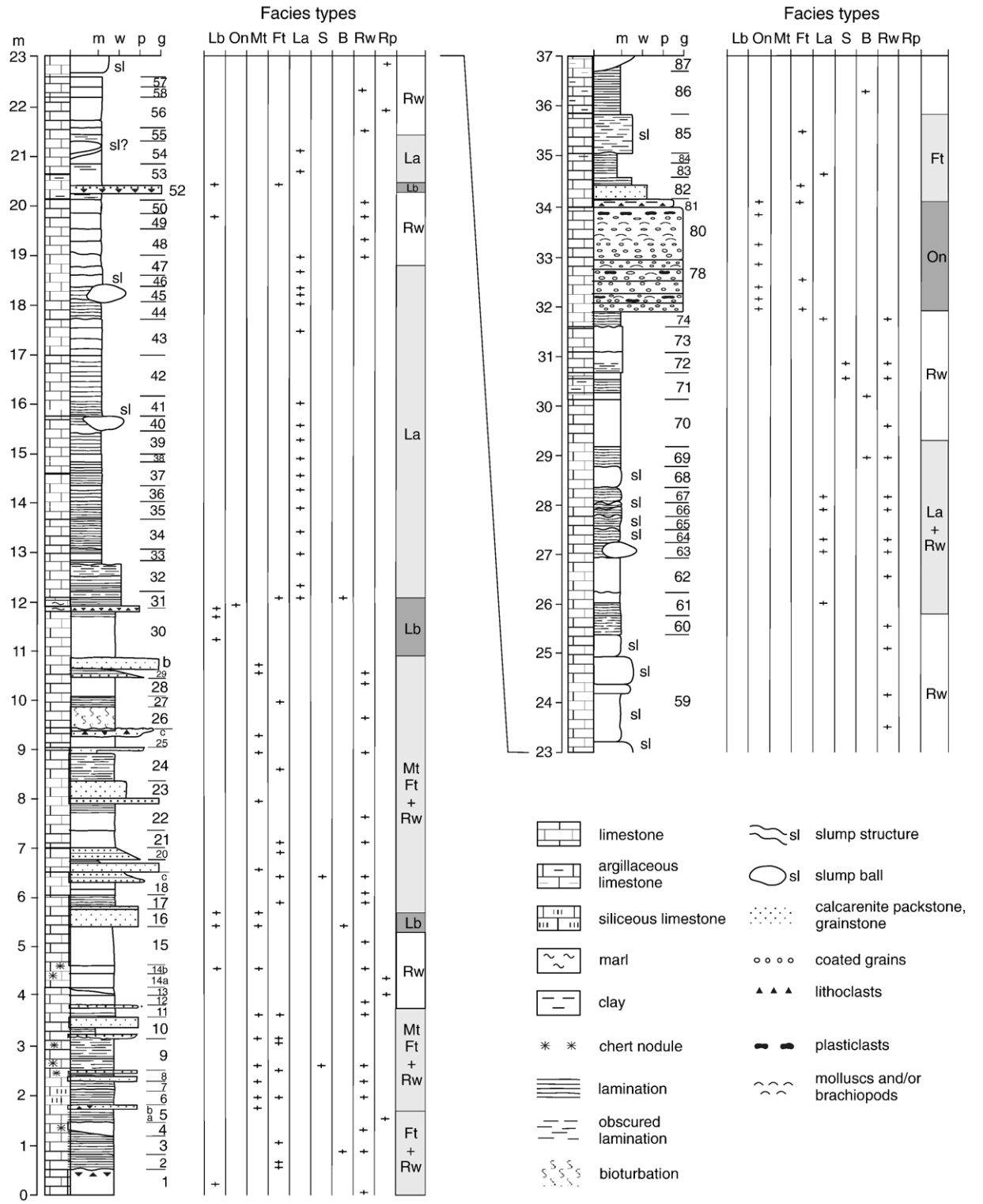

Fig. 3. Stratigraphic log of the Triassic–Jurassic boundary section at Csővár. For brief description of facies types, see Table 1. Abbreviations of facies types: Lb—lithoclastic-bioclastic grainstone/packstone, On—oncoidal grapestone, Mt—medium-grained calciturbidite, Ft—fine-grained calciturbidite, La—calcisilt-calcilutite laminite, S—sponge spicule wackestone, B—thin-shelled bivalve wackestone, Rw—radiolarian wackestone, Rp—radiolarian packstone. Successive stages of sedimentary basin evolution characterized by prevailing microfacies are shown on the right.

Table 1
Summary of characteristics and inferred depositional environment of the lithofacies types observed in the T–J boundary section at Csővár

Lithofacies type	Description (w: wackestone, p: packstone, gr: grainstone)	Interpreted depositional setting
Lithoclastic-bioclastic grainstone/packstone (Lb)	Fine-grained calcirudite to coarse-grained calcarenite gr, p crinoids, bivalves, foraminifera, ostracods, microproblematica, microbial crust fragments	Grain flow deposit—toe-of-slope
Oncoidal grapestone (On)	Coarse calcarenite gr, p, w brachiopods, bivalves, ostracodes	Toe-of-slope
Medium-grained calciturbidite (Mt)	Coarse to fine-grained, graded calcarenite p crinoids, molluscs, bethic foraminifera, microbial crust fragments, lithoclasts	High-density turbidity current—toe-of-slope
Fine-grained calciturbidite (Ft)	Fine calcarenite, peloidal p, and sponge spicule w alternate crinoids, molluscs, ostracodes, sponge spicules, radiolarians	Low-density turbidity current distal toe-of-slope—basin
Calcisilt-calcilutite laminite (La)	Laminitic: calcisilt and calcilutite alternate, w radiolarians, sponge spicules, thin-shelled ostracods, peloids	Low-density turbidity current—basin
Sponge spicule wackestone (S)	Calcisilt, calcilutite, sponge spicules, crinoids, filaments, radiolarians	Shallow basin
Thin-shelled bivalve wackestone (B)	Calcisilt, calcilutite, filaments, radiolarians, echinoderm fragments	Shallow basin
Radiolarian wackestone (Rw)	Calcisilt, calcilutite, radiolarians, sponge spicules filaments, echinoderm fragments	Deeper basin
Radiolarian packstone (Rp)	Calcisilt, radiolarians (very abundant), sponge spicules, echinoderm fragments	Deepest part of basin

might also reflect an extraordinary event (a "boundary-event horizon").

Above the boundary interval, various basinal facies prevail, indicating continuation of the long-term transgressive trend. A lack of platform-derived bioclasts is probably the consequence of drowning of adjacent platforms. However, crinoid fragments commonly occur both in the laminitic distal turbidites and the typical basinal facies. The top and the slope of the drowned platforms may have served as crinoid habitats.

The most striking lithological change in the Hettangian section is the appearance of redeposited oncoids and grapestones in a 2-m-thick, upward-thickening bundle (Beds 75–80), which is taken to indicate the end of the Rhaetian to earliest Hettangian third-order sequence. The coated grains were presumably formed on the top of drowned platforms during the late highstand to lowstand period and redeposited at the toe-of-slope during the lowstand.

The oncoidal beds are overlain by distal to very distal turbidites. In the upper part of the studied section, various basinal facies prevail (radiolarian, thin-shelled bivalve and sponge spicule facies) that reflect the second-order deepening upward trend. Bed 108 contains lithoclasts and redeposited oncoids and marks the base of the next cycle. However, recognition of metre-scale cycles in the upper part of the section is ambiguous.

4. Biostratigraphy

Macrofossils (ammonoids) and microfossils (radiolarians, foraminifera, conodonts) collected from the Csővár section formed the basis of biostratigraphic definition of the T–J boundary (Fig. 4). Emerging patterns of local faunal change are interpreted in the context of the end-Triassic extinction in the discussion section.

4.1. Radiolarians

Radiolarians from Csővár were first reported by Kozur and Mostler (1990), in a study on Hettangian saturnalids from the Northern Calcareous Alps, Bavaria. Kozur (1993) dated the upper part of the Várhegy Formation by the first appearance of *Relanus hettangicus*, which is considered the index for the Hettangian in the Northern Calcareous Alps (Kozur and Mostler, 1990). Other important Hettangian radiolarians from Csővár were also listed and illustrated, although the exact position of the samples was not provided (Kozur, 1993).

In the present study, >50 samples were processed by dissolving 0.7–1 kg of rock in acetic acid. Following standard laboratory extraction techniques (De Wever et al., 2001), the radiolarians were identified under a binocular microscope. The preservation is generally poor, and the radiolarian tests are commonly recrystallized. Identifiable radiolarians were extracted from Bed 4 and Bed 62 only, although Haas and Tardy-Filácz (2004) observed radiolarians and radiolarian calcite moulds in thin sections of numerous other layers.

Bed 4 contains abundant radiolarians, holothurians and sponge spicules. The radiolarians are all multicyrtid nassellarians belonging to the *Globolaxtorum tozeri*

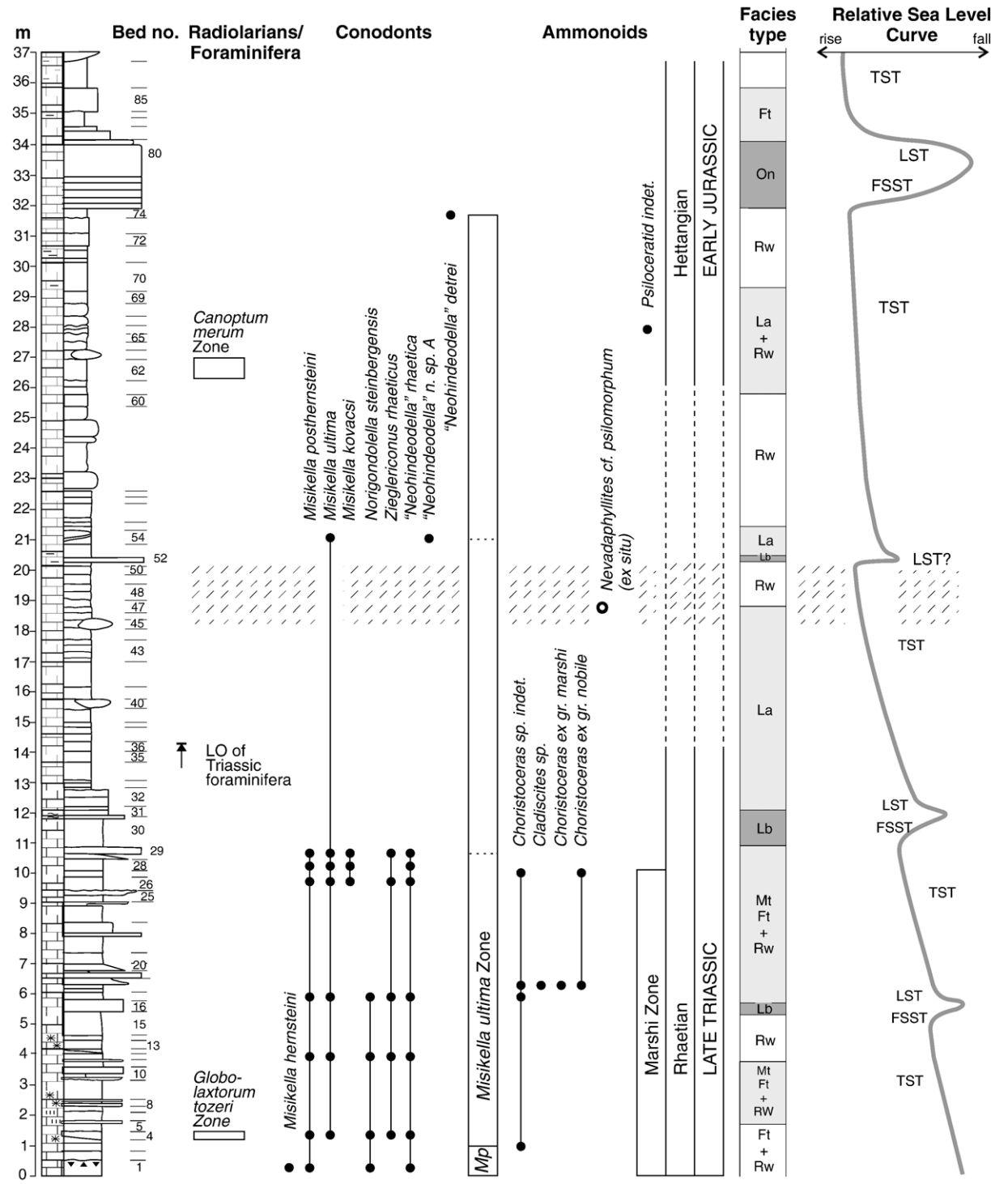

Fig. 4. Interpreted sea level history inferred from microfacies analysis and biostratigraphic distribution of the key fossil groups in the Csővár section, plotted against a simplified lithological log. Stippled pattern denotes level of the principal negative $\delta^{13}C$ excursion.

zone, indicating a Late Rhaetian age. The assemblage includes *Canoptum triassicum*, *Canoptum* spp., *G. tozeri*, *Laxtorum capitaneum*, *L. perfectum*, *L.* cf. *porterheadense*, *L.* spp., *Syringocapsa rhaetica* and a few other species too poorly preserved to identify. Fig. 5 illustrates the key radiolarian taxa.

In Bed 62, the spumellarians are more abundant than nassellarians. In the spumellarian fauna, saturnalids are dominant (incl. *Praehexasaturnalis*, *Palaeosaturnalis*, *Pseudoheliodiscus*, *Stauracanthocircus*, *Pseudacanthocircus*, *Spinoellipsella*), whereas patulibracchids (incl. *Paronaella*) and pantanelliids (incl. *Pantanellium*) also

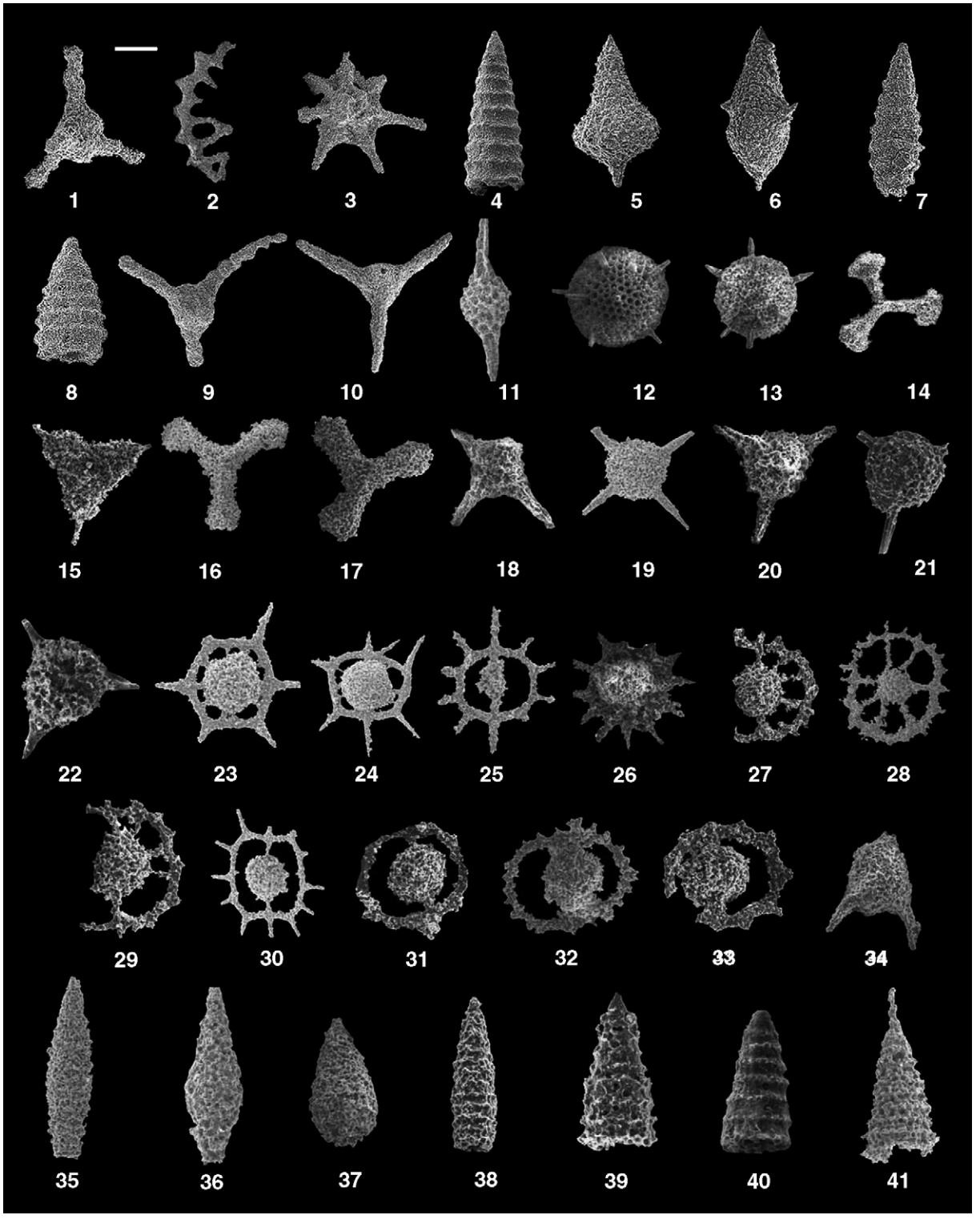

occur. Besides, the radiolarian fauna also contains rare entactiniids (*Charlottea* and *Tozerium*) and other genera (*Amuria*, *Plegmosphaera*, *Spongiomma*, *Praeorbiculiformella*, *Alievium*?, *Spongostaurus*, *Spongotrochus* and *Weverisphaera*). The nassellarian fauna is composed mainly of *Relanus* and *Canoptum*. Other genera (*Bipedis*, *Laxtorum* and *Syringocapsa*) are only rare elements.

The first zonation for the Early Jurassic radiolarian succession was developed based on western North American distribution data (Pessagno et al., 1987). Using this scheme, Bed 62 is assigned to the Hettangian Zone 05 (*Canoptum merum* Concurrent Range Zone, based on the presence of the species *Relanus* cf. *reefensis*). The lower boundary of this zone is defined by the first appearance of primary marker taxa *C. merum* and its upper boundary by the last appearance of *C. merum* and *Relanus reefensis*. The correlation with the Tethyan areas is difficult, because here *C. merum* has not been recorded in the lowermost Jurassic. However, it is said to occur in the Late Rhaetian strata of the Alps (Kozur and Mostler, 1990).

Alternatively, using the zonal scheme of Kozur and Mostler (1990), the radiolarian assemblage of Bed 62 is assigned to the *R. hettangicus* zone which is also regarded as Hettangian in age. This zone is confirmed here by coexistence of *R.* cf. *reefensis*, *Relanus longus* and *Pantanellium suessi*.

Further biostratigraphic constraints come from the genera *Bipedis* and *Tozerium*. Carter et al. (1998) identified their age range as Hettangian to Sinemurian. Also diagnostic is the presence of *Amuria impensa*, *Palaeosaturnalis liassicus*, *Praehexasaturnalis poultoni* and *Paronaella botanyensis* that co-occur in the lower part of the *Protokatroma aquila* zone and the upper part of the *Crucella hettangica* zone of Carter et al. (1998); this interval is dated as Middle and Late Hettangian.

An additional productive sample was collected from the south slope of Vár-hegy, above the measured section, ~ 40 m above Bed 62. Many species are represented by relatively well-preserved tests, although these are fragile and recrystallized. The radiolarian assemblage of this sample is similar to that from Bed 62 and it is also assigned to the Hettangian *R. hettangicus* zone.

In conclusion, radiolarian biostratigraphic constraints place the T–J boundary between Bed 4 (Late Rhaetian) and Bed 62 (Hettangian).

4.2. Foraminifera

Traditionally, studies of foraminifera from T–J boundary sections identified taxa from thin sections. This approach is here complemented with a study of isolated specimens, obtained by acetic acid extraction from 18 samples from between 2.3 and 45 m stratigraphic height.

Both methods yielded a diverse and abundant assemblage from the lower 12.5 m (up to Bed 32). Especially rich faunas, dominated by agglutinated forms, were recovered from Beds 30 and 31. Platform-derived forms are rare, although *Planiinvoluta carinata* is a notable exception that ranges through the entire section. *Triasina hantkeni*, a shallow water index species of the Rhaetian, has not been found, and other involutinids are

Fig. 5. Diagnostic radiolarians from the Csővár section. 1. *Paratriassoastrum*? sp.; Late Rhaetian, Bed 4; scale=50 μm. 2?*Haeckelicyrtium* sp. cf. *H. breviora* Sugiyama 1997; Late Rhaetian, Bed 4; scale=120 μm. 3. *Citriduma asteroides* Carter 1993, Late Rhaetian, Bed 4; scale=80 μm.4. *Canoptum triassicum* Yao 1982; Late Rhaetian, Bed 4; scale=75 μm. 5. *Globolaxtorum tozeri* Carter 1993; Late Rhaetian, Bed 4; scale=50 μm. 6. *Globolaxtorum*? sp.; Late Rhaetian, Bed 4; scale=60 μm. 7. *Laxtorum* sp. cf. *L. capitaneum* Carter 1993; Late Rhaetian, Bed 4; scale=60 μm. 8. *Laxtorum* sp.; Late Rhaetian, Bed 4; scale=60 μm. 9. *Livarella longa* Yoshida 1986; Late Rhaetian, Bed 4; scale=80 μm. 10. *Livarella valida* Yoshida 1986; Late Rhaetian, Bed 4; scale=80 μm. 11. *Pantanellium suessi* (Kozur and Mostler) 1990; Hettangian, Bed C; scale=80 μm. 12. *Amuria impensa* Whalen and Carter 1998; Early Hettangian, Bed 62; scale=100 μm. 13. *Spongiomma* ? sp.; Early Hettangian, Bed 62.5; scale=115 μm. 14. *Paronaella botanyensis* Whalen and Carter 1998; Early Hettangian, Bed 62; scale=180 μm. 15. *Paranoella* sp. 1; Early Hettangian, Bed 62; scale=180 μm. 16. *Paronaella* sp. 2; Early Hettangian, Bed 62; scale=180 μm. 17. *Paronaella* sp. 3; Early Hettangian, Bed 62; scale=180 μm. 18. *Spongostaurus* ? sp.; Early Hettangian, Bed 62; scale=170 μm. 19. *Spongotrochus* sp.; Hettangian, Bed C; scale=180 μm. 20. *Charlottea* sp.; Early Hettangian, Bed 62; scale=180 μm. 21. *Charlottea*? sp.; Early Hettangian, Bed 62; scale=180 μm. 22. *Tozerium*? sp.; Early Hettangian, Bed 62; scale=180 μm. 23. *Praehexasaturnalis kirchsteinensis* Kozur and Mostler, 1990; Early Hettangian, Bed 62; scale=180 μm. 24. *Praehexasaturnalis poultoni* Whalen and Carter 1998; Early Hettangian, Bed 62; scale=180 μm. 25. *Palaeosaturnalis liassicus* Kozur and Mostler, 1990; Early Hettangian, Bed 62; scale=180 μm. 26. *Pseudoheliodiscus* sp. cf. *P. alpinus*Kozur and Mostler, 1990; Early Hettangian, Bed 62; scale=180 μm. 27. *Pseudoheliodiscus* sp.; Early Hettangian, Bed 62; scale=180 μm. 28. *Pseudoheliodiscus* sp.; Early Hettangian, Bed 62; scale=180 μm. 29. *Stauracanthocircus assymetricus* Kozur and Mostler, 1990; Early Hettangian, Bed 62; scale=180 μm. 30. *Stauracanthocircus ruesti* Kozur and Mostler, 1990; Early Hettangian, Bed 62; scale=180 μm. 31. *Pseudoacanthocircus* sp. cf. *P. laevis* Kozur and Mostler, 1990; Early Hettangian, Bed 62; scale=180 μm. 32. *Spinoellipsella denispinosa* Kozur and Mostler, 1990; Early Hettangian, Bed 62; scale=180 μm. 33. *Spinoellipsella* sp. cf. *S. latispinosa* Kozur and Mostler, 1990; Early Hettangian, Bed 62.8; scale=180 μm. 34. *Bipedis* sp.; Early Hettangian, Bed 62; scale=80 μm. 35. *Canoptum* sp. 1; Hettangian, Bed C; scale=80 μm. 36. *Relanus hettangicus* Kozur and Mostler, 1990; Bed C; scale=80 μm. 37. *Relanus hettangicus* Kozur and Mostler, 1990; Early Hettangian, Bed 62; scale=120 μm. 38. *Relanus longus* Kozur and Mostler, 1990; Early Hettangian, Bed 62; scale=120 μm. 39. *Relanus* cf. *R. reefensis* Pessagno and Whalen 1982; Early Hettangian, Bed 62; scale=140 μm. 40. *Dictyomitrella* sp.; Early Hettangian, Bed 62; scale=80 μm. 41. Nassellarian indet. A *sensu* Whalen and Carter 1998; Hettangian, Bed C; scale=80 μm.

rare. Best represented are species of Nodosariidae, *Lenticulina* and *Dentalina*. The Rhaetian age of this interval is suggested by the occurrence of *Variostoma cochlea, V. coniforme, V. crassum*, *Ophthalmidium leischneri*, *Miliopora cuvillieri*, *Galeanella panticae*, *Ammobaculites rhaeticus* and *A. eomorphus*.

From 12.8 m, much impoverished assemblages were encountered. Few persisting Triassic species include *Aulotortus tenuis* and *A. tumidus*. From 25.6 to 34.7 m, an oligospecific association dominated by encrusting *P. carinata* occurs, except for facies-controlled assemblages of abundant smooth, elongated forms (*Eoguttulina*, *Ramulina* and *Dentalina*) in laminated beds at 29 and 30.4 m. The latter assemblage, which is interpreted to indicate relatively deeper (neritic to bathyal) environments, re-occurs in lesser abundance above 34.7 m. *Involutina liassica*, a diagnostic Jurassic species, first appears near the top of the section in Bed 119 at 52 m.

4.3. Conodonts

The stratigraphically lowest conodont collection (Bed 1) contains long-ranging *Norigondolella steinbergensis* and representatives of two *Misikella* species, *M. hernsteini* and *M. posthernsteini*. Fig. 6 illustrates the key conodont taxa. Recovered ramiform elements are assignable to *Norigondolella* (Orchard, 2005), and to the form species *Chirodella dinodoides* (= M element) and *Neohindeodella rhaetica* (= S_{1-3} elements); the latter show variation in the orientation of the cusp and the inturning of the distal end of the anterior process. Elements resembling these ramiform elements have been reconstructed as parts of both *Algherella* Bagnoli et al. (1985) and *Ellisonia dinodoides* sensu Koike (1994) and are long ranging through the Triassic. In the present collections, it is quite likely that they form part of the multielement *Misikella* apparatus. The conodont association corresponds to the lower part of the *M. posthernsteini* Assemblage Zone of Kozur and Mock (1991).

Stratigraphically higher collections from 1.7 m (Bed 4) through 10.4 m (Bed 29) are assigned to the *M. ultima* zone of Kozur and Mock (1991) based on the appearance of the zonal nominal species, although it is subordinate to *M. posthernsteini* throughout this interval. At 9.5 m (Bed 26) and 10.4 m (Bed 29), *Misikella kovacsi* n. sp. is differentiated: this element is rare but might help identify the higher parts of the *M. ultima* zone. *Zieglericonus rhaeticus* and an association of ramiform elements assigned to *Grodella delicatula* sensu formo (= S_{1-2} element), *Hindeodella andrusovi* s.f. (= S_{3-4} elements, with variable inturning of anterior process) and *Metaprioniodus* sp. s.f. (= M elements) also appear and range through the *M. ultima* zone. The ramiform elements are unlikely to be part of multielement *M. ultima* and are tentatively assigned to multielement *Zieglericonus*.

Single specimens of *M. ultima* and "*Neohindeodella*" sp. were recovered from 20.9 m (Bed 54), whereas Bed 74 at 31.7 m yielded "*Neohindeodella*" *detrei*. The latter record may support the suggestion of Kozur (1993) that at least one conodont lineage survived into the earliest Jurassic.

4.4. Ammonoids

The studied section yielded only scarce macrofossils, among which the ammonoids are the most useful for constraining the T–J boundary. Important finds were illustrated by Pálfy and Dosztály (2000) and their ranges and zonal assignments documented by Pálfy et al. (2001). Poor preservation hinders firm identification, but *Choristoceras* spp. from the lowest 10 m does indicate the *marshi* zone and a latest Rhaetian age. The T–J boundary interval only yielded *ex situ* phylloceratids. The suggestion of Guex et al. (2004) that a well-preserved specimen, previously identified as *Nevadaphyllites psilomorphum*, represents a Triassic *Rhacophyllites* is rejected on the basis of its juraphyllitid suture. The lowest Jurassic psiloceratid ammonoid found in place occurs at 28.5 m (Bed 66). *Waehneroceras* sp. collected at the top of the measured section (Bed 124) indicates a middle Hettangian age.

5. Stable isotope geochemistry

Previous studies established the presence of a negative $\delta^{13}C$ peak at the T–J boundary at Csővár

Fig. 6. Diagnostic conodonts from the Csővár section. Type numbers of the Geological Survey of Canada are prefixed GSC. All figures ×120. Abbreviation s.f. = sensu formo. 1. *Misikella hernsteini* (Mostler). P_1 element GSC 120172, Bed 1. 2,3. *Misikella posthernsteini* Kozur and Mock. P_1 elements. 2. GSC 120173, Bed 17; 3. GSC 120174, Bed 4. 4–7, 9. *Misikella ultima* Kozur and Mock. P_1 elements. 4. GSC 120175, Bed 4; 5. GSC 120176, Bed 4; 6. GSC 120177, Bed 54a; 7. GSC 120178, Bed 28; 9. GSC 120179, Bed 4. 8. *Misikella kovacsi* n. sp. P_1 element GSC 120180, Bed 29. 10, 13, 18. *Norigondolella steinbergensis* (Mosher). 10. P_1 element, GSC 120181, Bed 1; 13. P_2 element GSC 120182, Bed 1; 18. M element, GSC 120183, Bed 4. 11, 15, 17, 21. *Neohindeodella rhaetica* Kozur and Mock s.f. S_{1-4} elements of *Misikella*? 11. S_{1-2} element GSC 120184, Bed 4; 15. S_{3-4} element GSC 120185, Bed 12; 17 S_{1-2} element GSC 120186, Bed 4; 21. S_{3-4} element GSC 120187, Bed 4. 12.S_0 element of *Misikella*? GSC 120188, Bed 4. 14. *Epigondolella* sp. Juvenile P_1 element GSC 120189, Bed 4.16. '*Metaprioniodus*' sp. s.f. M element of *Zieglericonus*? GSC 120190, Bed 4. 19, 24. '*Hindeodella*' *andrusovi* Kozur and Mostler s.f. 19. S_{3-4} elements of *Zieglericonus*? S_4 element GSC 120191, Bed 4; 24. S_3 element GSC 120192, Bed 17. 20. '*Chirodella*' *dinodoides* (Tatge) s.f. M element of *Misikella*? GSC 120193, Bed 4. 22. *?Zieglericonus* sp. A. P_2? element GSC 120194, Bed 4. 23. '*Grodella*' *delicatula* (Mosher) s.f. S_{1-2} element of *Zieglericonus*? GSC 120195, Bed 4. 25. '*Neohindeodella*' n. sp. A s.f. S element GSC 120196, Bed 54a. 26. '*Neohindeodella*' cf. *detrei* Kozur and Mock s.f. S element GSC 120197, Bed 74. 27. *Zieglericonus rhaeticus* Kozur and Mock P_1 element GSC 120198, Bed 4.

(Pálfy et al., 2001) and elsewhere, and suggested that the anomaly is useful as a global correlation tool (Ward et al., 2001; Hesselbo et al., 2002; Guex et al., 2004; Galli et al., 2005). Recognition of complexities of $\delta^{13}C$ records and the governing processes (e.g. Ward et al., 2004) requires additional, high-resolution studies and careful evaluation of data so that diagenetically altered material is identified and avoided. To augment the isotopic data published in Pálfy et al. (2001), new sets of samples were collected from the T–J boundary interval of the same section (here referred to as the "main section") and from a parallel stratigraphic section ~ 10 m to the east (referred to as section B). Sampling was also extended to the higher part of the main section (above 38 m, Fig. 7).

Carbon and oxygen isotope compositions of drilled carbonate samples were determined using the conventional H_3PO_4 digestion method (McCrea, 1950). $^{13}C/^{12}C$ and $^{18}O/^{16}O$ ratios of CO_2 generated were measured with a Finnigan MAT delta S mass spectrometer at the Institute for Geochemical Research in Budapest. The results are expressed in the δ-notation [$\delta=(R_1/R_2-1)\times 1000$] where R_1 is the $^{13}C/^{12}C$ or $^{18}O/^{16}O$ ratio in the sample and R_2 the corresponding ratio of the standard (V-PDB for C and V-SMOW for O), in parts per thousand (‰). Reproducibilities are better than ±0.15‰.

Stratigraphic trends of $\delta^{13}C_{carb}$ and $\delta^{18}O_{carb}$ are plotted in Fig. 7, and include data from Pálfy et al. (2001) together with new data reported in the present study. Relationships between the $\delta^{13}C$ and $\delta^{18}O$ data are also presented in Fig. 8A. As the $\delta^{13}C$ excursion in the boundary interval appeared in both carbonate and organic matter it has been interpreted as a primary signal (Pálfy et al., 2001). A number of samples show a more marked $\delta^{18}O$ shift associated with moderate ^{13}C-depletion in the carbonate, which is likely a trend related to diagenesis. For a higher resolution analysis, the section of Pálfy et al. (2001) (our "main section") was re-sampled and the carbonate analysed for C and O isotope compositions. The analyses yielded a slightly different pattern (Fig. 8A). It is important to note that, during re-sampling, a network of calcite veins was

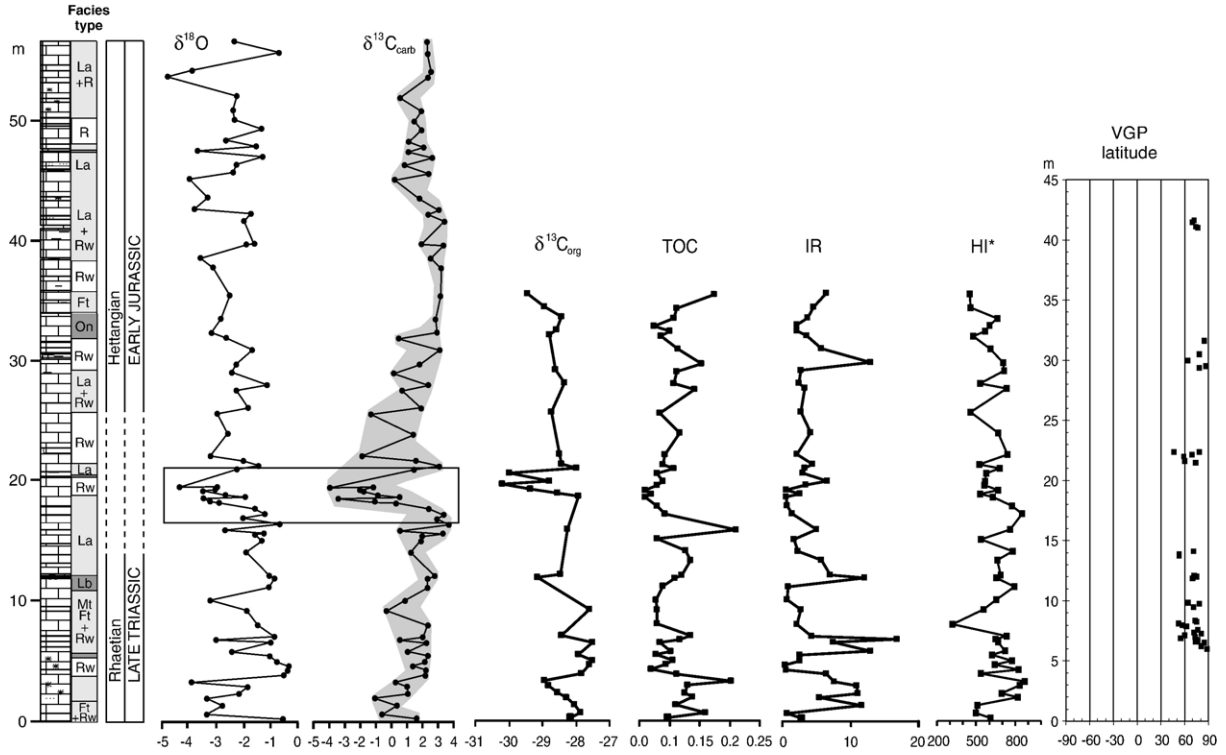

Fig. 7. Stable isotope, organic geochemical and palaeomagnetic characteristics of the main T–J boundary section at Csővár. C and O isotopic compositions of carbonate (in ‰ relative to V-PDB) shown include the data reported by Pálfy et al. (2001) and new data (but excluding diagenetically altered samples with $\delta^{18}O<-5‰$). Box marks the interval of principal negative carbon isotope anomaly, reproduced in parallel section B, as shown in Fig. 9. Changes in $\delta^{13}C_{org}$, insoluble residue (IR), total organic carbon (TOC) and hydrogen index (HI*) are from Pálfy et al. (2001). VPG latitudes of samples retaining primary remanent magnetization. All data plotted along the measured stratigraphic section showing prevailing lithofacies (for key, see Fig. 3 and Table 1).

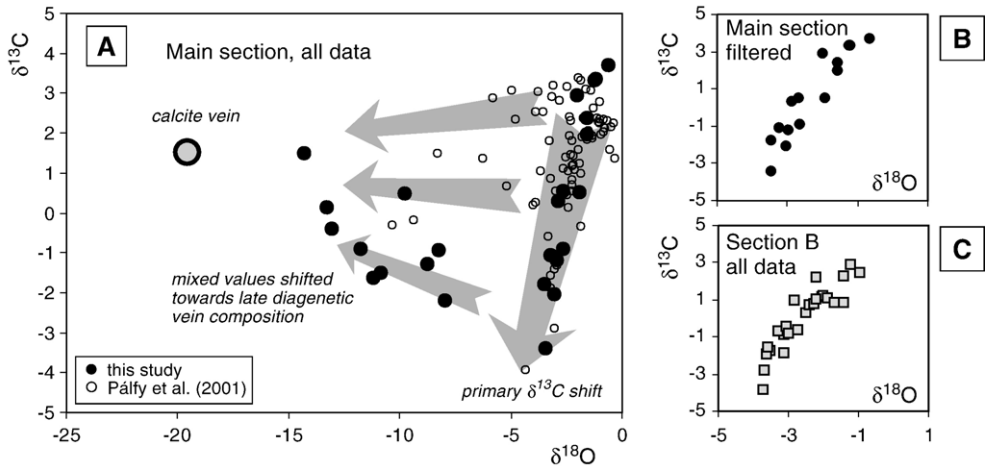

Fig. 8. Cross plots of $\delta^{13}C_{carb}$ vs. $\delta^{18}O$ values (in ‰ relative to V-PDB). (A) All data from the main section obtained in this study (filled circles) compared with the data reported in Pálfy et al. (2001) (empty circles). Arrows indicate the primary carbon isotope shift as well as the effect of mixing of late diagenetic calcite vein material and primary carbonate. (B) Filtered data ($\delta^{18}O<-5$‰) from the T–J boundary carbon isotope excursion interval of main section (16 to 21 m above base). (C) All data from T–J boundary carbon isotope excursion interval of section B. Note similarity of B and C.

observed (obvious signs of late-stage alteration). The isotopic compositions of a large calcite vein, ~ 10 cm in width (shown in Fig. 8A), help explain the observed variations as mixing of primary carbonate and the vein material (shown by arrows in Fig. 8A). Obviously, the re-sampled material of the main section has been affected by late-stage fluid circulation. The negative $\delta^{18}O$ shift in many of the samples can be attributed to the presence of sub-millimetre veins in the bulk samples. However, if only those carbonate samples are considered whose $\delta^{18}O$ values are higher than −5‰, their $\delta^{13}C$ and $\delta^{18}O$ values reproduce the primary isotope shift reported in Pálfy et al. (2001) (Fig. 8A), suggesting that these samples have not been affected by the calcite vein formation. For confirmation of the isotopic trends, high-resolution sampling was carried out from a parallel section where calcite veins are absent and a diagenetic overprint could be avoided.

Section B is stratigraphically correlated with the main section but is superior for stable isotope stratigraphy for the apparent lack of calcite veins. The $\delta^{13}C_{carb}$ and $\delta^{18}O_{carb}$ values of section B show a close correlation (Fig. 8C), in a similar manner to the filtered samples of the main section (Fig. 8B). The $\delta^{13}C_{carb}$ values decrease to −4.5‰, supporting the interpretation that section B indeed represents the boundary layers containing the $\delta^{13}C$ excursion detected from the main section (Pálfy et al., 2001 and this study). Section B not only preserved the primary stable isotope signal more reliably, but its higher resolution sampling also revealed that the negative excursion is composed of a succession of up to five cycles of negative shifts followed by rebounds (Fig. 9).

Negative $\delta^{13}C$ shifts were documented not only in the carbonate, but also in the organic matter (Pálfy et al., 2001). Pronounced negative shifts in the organic matter

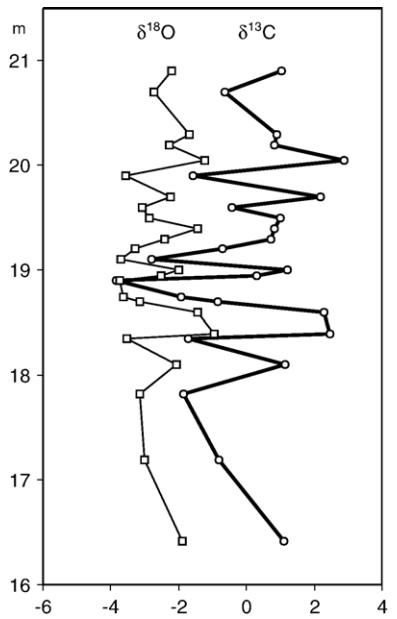

Fig. 9. High-resolution $\delta^{13}C_{carb}$ and $\delta^{18}O$ data (in ‰ relative to V-PDB) from the T–J boundary interval in section B. Stratigraphic position is based on correlation with the main section and expressed in metres above its base.

would be difficult to explain with diagenesis, and the correlated change is interpreted as evidence for a primary feature. The primary nature of the C–O isotope variations is also supported by the good agreement with the initial and unaltered isotope compositions established elsewhere for latest Triassic rocks ($\delta^{13}C = 2‰$ to 4‰, $\delta^{18}O = -4‰$ to $-2‰$, Ward et al., 2004; Galli et al., 2005).

6. Organic geochemistry

The extremely low amount of organic matter (OM) in the studied rocks necessitated that both Rock-Eval (RE) pyrolyses and $\delta^{13}C_{org}$ analyses were carried out on acid-insoluble residue (IR) after removal of carbonate. RE values were determined on a Delsi Oil Show Analyzer using standard pyrolysis procedures (Espitalié et al., 1986; Bordenave et al., 1993). First the sample was heated at moderate temperature, during which time the hydrocarbon already generated within the source rock (and/or the allochtonous hydrocarbons) was volatilized (S_1 peak: hydrocarbonaceous compounds released from 1 g sample). Then, the hydrocarbons cracked from the organic matter at progressively increased temperature were measured as the S_2 peak (hydrocarbonaceous compounds yielded by 1 g sample). The inert organic carbon (i.e. that produces no hydrocarbon), remaining after recording the S_1 and S_2 peaks, was measured by oxidation under an air flow at 600 °C and labeled S_4. The total organic carbon content was computed from S_1, S_2 and S_4. The temperature corresponding to the maximum of the S_2 peak (T_{max}) is used for evaluation of the thermal maturity.

Results of the Rock-Eval pyrolysis and amounts of IR are listed in Table 2 and displayed in Fig. 7. The studied rocks are poor in OM; TOC is less than 0.1% for all but two samples. Hydrogen index values (HI, defined as the carbon-normalized S_2) are higher than 400 mg hydrocarbon/g of organic carbon for most of the samples and reveal predominantly marine, hydrogen-rich OM.

T_{max} values, ranging between 430 and 442 °C, are typical for marginally mature hydrogen-rich OM, and indicate that kerogens of the studied samples have already realised a significant part of their hydrocarbon potential. S_1 peaks are surprisingly high compared to S_2 peaks in most of the samples, but the low TOC values support the assumption that they represent autochtonous hydrocarbons and not allochtonous ones. Consequently, HI* (defined as $(S_1+S_2)/TOC$) provides more reliable information about hydrogen richness of the OM than does HI (defined as S_2/TOC).

Table 2
Average values of IR, Rock-Eval data and $\delta^{13}C_{org}$ in successive intervals of different lithofacies in the Csővár T–J boundary section

Bed no. (sample no.)	IR (%)	TOC (%)	HI* (mg HC/g TOC)	$\delta^{13}C_{org}$ (‰)	Facies
82–85 (2/2)	5.57	0.093	452	−29.2	Ft
75–80b (4/3)	2.91	0.045	577	−28.68	On
70–72 (2)	9.36	0.084	657	n.d.	Rw
61–69 (3/2)	2.83	0.07	659	−28.47	La+Rw
55–60 (4/3)	3.38	0.046	599	−28.55	Rw
53–54 (2/2)	**3.18**	**0.044**	**631**	**−28.98**	**La**
47–50 (4/4)	**3.32**	**0.025**	**584**	**−29.23**	**Rw**
44–45 (2/1)	**0.65**	**0.02**	**702**	**−27.94**	**La**
31–43 (7/3)	5.06	0.075	706	−28.61	La
30 (1)	0.9	0.039	794	n.d.	Lb
17–28 (7/3)	6.73	0.047	615	−27.86	Mt-Ft+Rw
16B (1/1)	2.62	0.028	626	−27.93	Lb
13A–15 (3/2)	1.24	0.04	750	−27.55	Rw
1A–11 (8/8)	7.1	0.09	675	−28.31	Mt-Ft+Rw

Bold face marks the T–J boundary interval. Sample numbers in parentheses in the first column refer to number of samples analysed by Rock-Eval pyrolysis/number of samples analysed for $\delta^{13}C_{org}$.

The coupling of high hydrogen content and extremely low amount of OM suggests that the labile OM was probably protected by inclusion in biogenic carbonate shell material. Physical protection of OM by shell calcite was reported from 2 Ma old deep-sea planktonic foraminifera that contain 1–2 μmol/g amino acids not destructible by bleaching with NaOCl and extractable only after dissolution in HCl (Stathoplos and Hare, 1993). Salmon et al. (1997) demonstrated that 0.1-mm-thick clayey layers intercalated with organic-lean carbonates could play a key role in the formation of type II kerogen via sorptive preservation. The importance of this preservation process was also recognized in recent sediments (Hedges and Keil, 1995).

Understanding the C-isotope excursion requires consideration of factors that control the geochemistry of the marine organic carbon pool. Types of organic precursors vary in different types of depositional environment. Transformations of the OM during early diagenesis are also influenced by the environment. The abundance and composition of OM, the amount of IR, and the relationship to lithofacies and $\delta^{13}C_{org}$ are discussed. Average TOC, HI* and IR values were calculated for the different turbiditic and basinal intervals and are listed in Table 2.

Turbidites (Beds 1–11 and 17–28) contain OM somewhat less rich in hydrogen relative to basinal sediments (Beds 13–15 and 31–43) below the T–J boundary interval. HI* shows significant negative correlation with $\delta^{13}C_{org}$ in turbidites, while no such correlation is found in basinal sediments (Fig. 10).

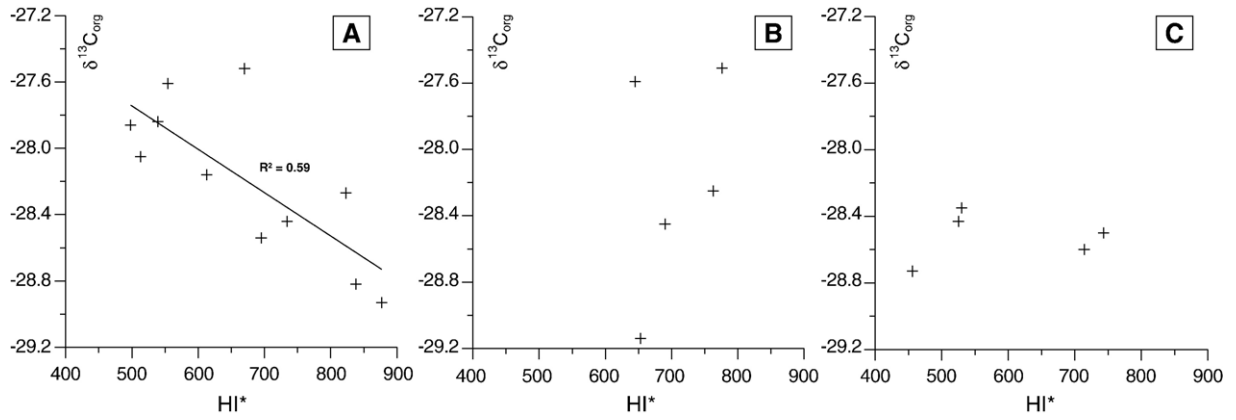

Fig. 10. Facies control on organic geochemical characteristics illustrated on cross plots of HI* vs. $\delta^{13}C_{org}$. (A) Data from turbiditic lithofacies below the T–J boundary principal isotope excursion. (B) Data from basinal lithofacies below the T–J boundary principal isotope excursion. (C) Data from basinal lithofacies above the T–J boundary principal isotope excursion.

The differences between turbidites and basinal sediments indicate that a significant portion of the OM of turbidites consists of isotopically heavy terrestrial components, relatively poor in hydrogen, whereas their contribution is smaller in basinal sediments. The first negative $\delta^{13}C_{org}$ shift near the base of the main section (Fig. 7, Beds 1–8), accompanied by a clear upward increase of HI* is explained by this mixing process, i.e. by a gradual upward decrease of terrestrial contribution to OM.

Concurrently with the principal negative $\delta^{13}C_{org}$ excursion, a significant upward decrease of TOC content and a drop in HI* is observed in the lower part of the T–J boundary interval (Fig. 7). Both the TOC and $\delta^{13}C_{org}$ return to pre-excursion values in the upper part of the T–J boundary interval, whereas HI∗ shows only a slight increase (Fig. 7).

Since Rock-Eval pyrolysis was carried out on only two turbidite samples from above the T–J boundary interval, a reliable comparison between turbidites and basinal sediments cannot be made. However, in basinal sediments, the value of HI* shows no correlation with $\delta^{13}C_{org}$ (Fig. 10C), indicating that there was no significant contribution of terrestrial organic components in the basinal facies.

Average TOC and HI* values show that basinal strata above the T–J boundary interval (Beds 55–72) contain kerogen impoverished in hydrogen relative to similar facies below the T–J boundary interval (Table 2). The lack of correlation between HI* and $\delta^{13}C_{org}$ argues against a significant contribution of terrestrial organic compounds; therefore, the lower average HI* values are tentatively interpreted to mark a stronger early diagenetic degradation (perhaps due to higher oxygen content of the bottom water) compared to the OM in basinal sediments below the T–J boundary interval.

7. Magnetostratigraphy

The latest Triassic–earliest Jurassic time interval was characterized by essentially normal polarity of the Earth's magnetic field. However, in one of the few sections (lacustrine sediments in the Newark Basin, eastern North America) that is apparently continuous across the boundary, a detailed magnetostratigraphic study revealed a short reversed polarity zone of latest Rhaetian age (Kent et al., 1995). A possibly correlative short reversed polarity interval is documented near the T–J boundary at St Audries' Bay, England (Hounslow et al., 2004). In the present study, an attempt was made to detect this reversed polarity zone at Csővár, to establish independent correlation with other continuous sections.

For the palaeomagnetic measurements, 54 cores were drilled representing 44 m of the section, with special attention to the T–J boundary interval. The samples were oriented in the field using a magnetic compass. The cores were cut into standard size specimens and their palaeomagnetic measurements, including the study of the magnetic minerals, were carried out in the Palaeomagnetic Laboratory of Eötvös Loránd Geophysical Institute. As a result of AF, thermal and combined demagnetization study of the magnetic mineralogy, we achieved the following results.

Most samples with well-defined remanence direction have weak, but stable natural remanent magnetization on demagnetization, indicating normal polarity (Fig. 7). The dominant magnetic mineral is magnetite; goethite is

absent. The mean direction is $D=289°$, $I=38°$, $k=16$, $\alpha_{95}=7°$ in geographic, and $D_c=300°$, $I_c=43°$, $k=18$, $\alpha_{95}=7°$ in tectonic coordinate system. These directions fit well an earlier defined direction for a locality of similar age nearby ($D_c=291°$, $I_c=49°$, $k=20$, $\alpha_{95}=10°$; Márton, 1998), both suggesting that the Csővár area suffered ~ 70° counterclockwise rotation after the Late Triassic (Fig. 11). Samples collected from the T–J boundary interval between the biostratigraphically constrained highest Triassic and lowest Jurassic strata are of reversed polarity. However, the mean palaeomagnetic direction calculated from the reversed samples ($D=189°$, $I=-65°$, $k=165$, $\alpha_{95}=5°$ in the geographic system) is characterized by about 9° clockwise rotation (Fig. 11). Since the tectonic unit comprising the Csővár area is characterized by counterclockwise rotated declinations up to 14.5 Ma (Márton and Pécskay, 1998), the remanence of reversed polarity at the Várhegy section cannot be primary. The secondary formation of this remanence is also supported by magnetic mineralogy experiments and microscopy observations, both revealing a considerable amount of goethite (apparently an alteration product of pyrite), which is the carrier of the palaeomagnetic signal in the reversed polarity samples, as proved by the thermal demagnetization of the natural remanent magnetization.

In summary, the T–J boundary segment of the Csővár section is mostly of normal polarity (primary

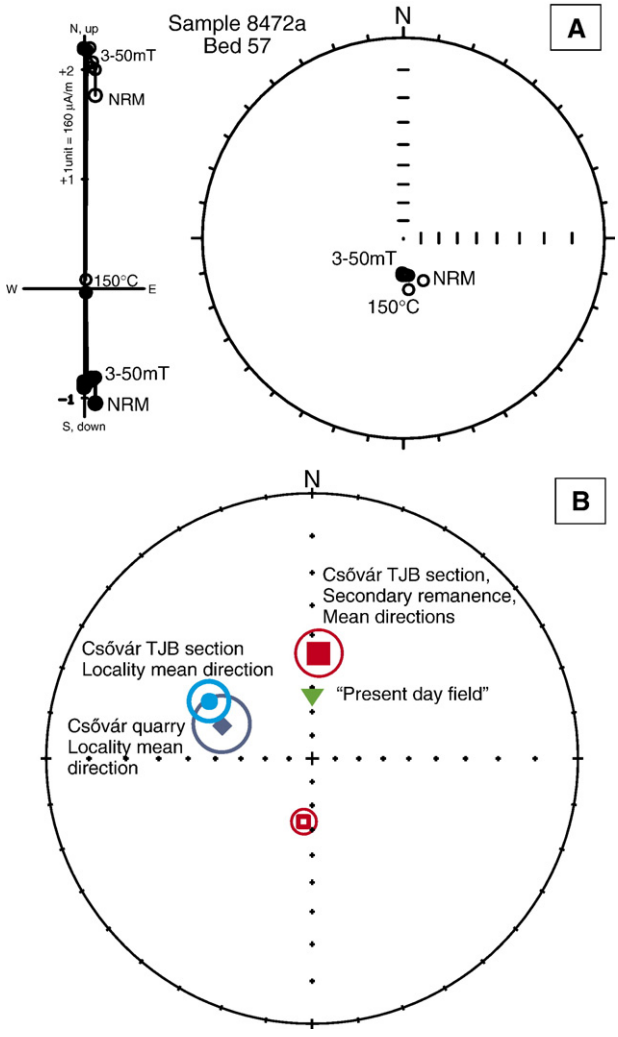

Fig. 11. (A) Typical demagnetization behaviour of a selected sample of reversed polarity from the T–J boundary section at Csővár, and directions of its secondary remanent magnetization on a stereographic projection. (B) Palaeomagnetic directions of primary remanence of normal polarity and secondary remanence of both normal and reversed polarities from the Csővár T–J boundary section, plotted on a stereographic projection. Mean direction of from Late Triassic strata from the nearby Csővár quarry and direction of present day field shown for comparison.

remanence). Although a reversed polarity zone is recognized close to the expected boundary, it cannot be attributed to primary field reversal at the end of the Triassic, for the direction of the natural remanence corresponds to a young Neogene palaeomagnetic direction expected for the Csővár area. Distinguishing between Mesozoic and Neogene palaeomagnetic signals was possible because our magnetostratigraphy was based on fully oriented samples and previous studies had established the direction of Triassic remanent magnetization for the Csővár area. Otherwise, the reversed magnetization could have easily been regarded a field reversal at the T–J boundary, leading to misinterpretation.

8. Clay and micromineralogy

From the studied section, 12 samples were analyzed for clay minerals, including a clay-rich layer (Bed 31) in the uppermost Triassic, considered as a possible tuff layer in the preliminary assessment of the section. Verification of a tuff layer close to the boundary would be significant for the reconstruction of the event. In addition, limestone and marl layers were sampled.

After pulverization, the carbonate content was dissolved by 5% acetic acid. X-ray powder diffraction (XPD) was carried out on all of the insoluble residues. For clay minerals, the residues were cut at 10 μm using Stokes law. Oriented samples were prepared on glass plates. After the X-ray measurements, ethylene-glycol treatment was applied to facilitate determination of the mixed and interlayered clay minerals. The diffractograms of the clayey layer and that of the residual insoluble clay fractions of the other layers (limestone, marl) were similar: beside the dominant quartz, a kaolinite-group mineral ($d001 = 7.1$ Å), an illite-muscovite phase ($d001 = 10$ Å) and an illite-smectite interstratified phase ($d001 = 11.7$ Å) were identified. No montmorillonite reflections were detected. The smectite content in the illite-smectite mixed and interlayered phase was determined by using a modified version of the method of Reynolds and Hower (1970). The determined smectite/illite content is 25/75%.

The data show no volcanic component in any of the samples and no significant change throughout the section. The only variable is the carbonate content which acts as a diluting factor against relatively constant clay sedimentation. Therefore the supposed tuff bed (Bed 31) is shown to be only a clay-rich layer, formed either by condensation or an increase in clay flux.

For assessment of micromineralogy, 39 samples were collected. Heavy liquid separation was applied to the insoluble residue excluding the clay fraction of <63 μm. From the heavy mineral fraction, all of the allogenic grains were handpicked under a stereomicroscope. The grains were observed by stereo- and petrographic microscope, and analyzed with a wavelength dispersive microprobe. The identified minerals include two types of almandine, grossular, andradite, dravite, staurolite, Mg-hornblende, rutile, ilmenite, titanomagnetite, magnetite and gold.

Despite the large sample size (ca. 1 kg), there were only few allogenic grains and some samples were completely barren. Although the small number of grains precludes the use of regular statistical methods to infer the parent rock and provenance area, the mineral association allows a reliable qualitative assessment. This association is thought to have derived from an eroding metamorphic area, with meso-metamorphic rocks of sedimentary origin, contact metamorphic rocks and magmatic rocks.

The Triassic and Jurassic parts of the section are similar in composition, but in the Jurassic part, in Beds 69–70 and 84–85 a few metres above the boundary, a significant increase of the allotigenous grains is demonstrated. This increase might indicate a climate change towards elevated humidity and increased runoff.

9. Discussion

9.1. Biotic change across the T–J boundary

Fossil distribution across the T–J boundary in the Csővár section is interpreted as a local record of the end-Triassic biotic crisis that affected differentially the various fossil groups. The ammonoid, radiolarian, foraminifera and conodont record, although of different quality and resolution, reflects the evolutionary history of these organisms.

Although only two levels yielded radiolarian assemblages, they are confidently assigned to the latest Rhaetian *Globolaxtorum tozeri* (Bed 4) and the earliest Hettangian *C. merum* or *R. hettangicus* (Bed 62) zones, respectively. The two assemblages share no common species. Such high turnover rate suggests that radiolarians suffered severe extinction at the end of Triassic. Similar observations have been made in the eastern and western Pacific (Japan and Canada, Carter and Hori, 2005). Congruent Panthalassan and Tethyan records suggest a global radiolarian event, and a significant species-level extinction that is one of the most prominent manifestations of the end-Triassic crisis. Poor preservation due to recrystallization elsewhere in the

section precludes reconstruction of the detailed pattern of extinction and recovery.

Change in the foraminiferan fauna is more subdued and any possible extinction signal is masked by facies-controlled differences through the section. The distribution of isolated specimens across the T–J boundary is studied here for the first time and provides a valuable complement to thin section observations. A moderate diversity is recorded in productive samples up to Bed 36, which corresponds to the last occurrence of characteristic Triassic forms. Assemblages from higher samples (with the exception of Bed 69) are impoverished, lack any diagnostic Triassic elements and consist of long-ranging taxa rather than newly evolved Jurassic species. Unfortunately, the number of acid-extracted specimens is as yet inadequate for statistical treatment. Local records from other T–J boundary sections register extinctions only in shallow marine platform environments, e.g. in the Zu Limestone of the Southern Alps, exemplified by the disappearance of *T. hantkeni* (Lakew, 1990). Elements of the fauna typical of platforms are rare at Csővár and *Triasina* is missing. Our record suggests that foraminiferan extinction in deeper water, basinal environments was less severe than in shallow water.

Conodonts have been considered victims of the T–J boundary extinction (e.g. Aldridge, 1988). As a Palaeozoic holdover group, they were in decline throughout the entire Late Triassic. In the Csővár section, a rather low diversity is maintained in the Late Rhaetian. Fifteen form species, thought to represent nine multielement species, occur up to Bed 29 (10.4 m). Only one or two taxa are recorded at two levels much higher upsection (20.9 and 31.7 m). Both of these occurrences are from above the principal carbon-isotope excursion; the higher one is also above undoubtedly Jurassic radiolarians and ammonoids. Conodonts above the 'initial' T–J boundary carbon isotope anomaly are also known in the St Audries' Bay section (Swift, 1989; Hesselbo et al., 2002). Our findings support the idea that some conodonts survived into the earliest Jurassic, a view that was postulated by Kozur (1993) but which hitherto lacked firm, independent stratigraphic evidence.

Microfacies analysis also supports the notion that a marked reduction in biotic components occurs above Bed 31, at the base of the latest Triassic sedimentary cycle (Haas and Tardy-Filácz, 2004).

9.2. Geochemical evidence for environmental change across the T–J boundary

A slight decrease in TOC followed by an increase observed in the T–J boundary interval may reflect a fall in planktonic production (C_{prod}), followed by a recovery. This interpretation is consistent with the severe radiolarian extinction. Since a drop in C_{prod} would have resulted in a relative enrichment of terrestrial OM components, changes in HI* may be explained by an increased and decreased contribution of H-poor terrestrial organic components to OM. However, since basinal sediments are overall poor in terrestrial organic components, the relative enrichment of the latter is not sufficient to account for the magnitude of the drop in HI* in the lower part of the T–J boundary interval (from 850 to 550 mg HC/g TOC). Additional factors may include that the recovering planktonic community furnished OM less suitable for preservation than before the extinction, or that the oxygen content of the bottom water increased after the extinction. Both changes would have resulted in a stronger degradation of OM during early burial, reflected in a pronounced decrease of HI*. However, facies evidence in support of significant changes in bottom water oxygenation is lacking.

Several previous studies documented a negative $\delta^{13}C$ excursion at the T–J boundary (Pálfy et al., 2001; Ward et al., 2001; Hesselbo et al., 2002; Guex et al., 2004; Galli et al., 2005) and considered it as a global correlation tool. Some of the published data indicate that the boundary interval is marked by multiple $\delta^{13}C$ shifts. Our new data from the Csővár section further supports this observation. Although the upper part is characterized by sediment reworking which masks fine-scale (<1 m) $\delta^{13}C_{carb}$ variations, a second $\delta^{13}C_{carb}$ shift appears following the boundary peak at ~ 45 m (Fig. 7). An earlier excursion preceding the boundary (at ~ 2 m, Fig. 7) may be correlative to the smaller peak documented from St Audrie's Bay (Hesselbo et al., 2002), although a change in the ratio of terrestrial and marine OM may also account for the $\delta^{13}C_{org}$ shift in the St Audrie's Bay section. The fluctuations argue against a single, instantaneous cause (i.e. an impact event) and rather indicate periodic instability in the global carbon cycle.

High-resolution analysis of the T–J boundary strata in section B indicates that the boundary excursion is composed of a set of high-amplitude $\delta^{13}C_{carb}$ fluctuations (Fig. 9). In other studies where sampling resolution is similar to ours, published curves indicate the same phenomenon both in carbonate and organic matter (Hesselbo et al., 2002; Guex et al., 2004; Ward et al., 2004).

The Csővár data also show that the $\delta^{13}C$ fluctuations are correlated with $\delta^{18}O$ changes. Variations in $\delta^{18}O$ values can be attributed to changes either in temperature or the oxygen isotopic composition of seawater (i.e.

salinity change). A frequently cited process that can lead to rapid global $\delta^{13}C$ changes of a magnitude of about −2‰ to −6‰ is release of methane from gas hydrates most probably triggered by global warming (Dickens et al., 1995; Dickens, 2003; Hesselbo et al., 2000; Pálfy et al., 2001). The Earth was in a greenhouse climate state around the T–J boundary, therefore the possible effect of polar ice melting is unlikely. However, it is interesting to note that similar $\delta^{13}C$–$\delta^{18}O$ relationship was observed in alternating Pleistocene glacial–interglacial layers where methane release was proposed to be responsible for sudden changes in $\delta^{13}C$ (Kennett et al., 2000), although the magnitude of shifts is much lower than observed for the T–J boundary event. Another comparable event is the Paleocene–Eocene thermal maximum, associated with strong $\delta^{13}C$ and $\delta^{18}O$ shifts attributed to methane release during rapid warming (Dickens et al., 1995). Plotting the $\delta^{13}C$ and $\delta^{18}O$ data of both Kennett et al. (2000) and Dickens et al. (1995) reveals that the slope of the $\delta^{13}C$–$\delta^{18}O$ correlation is very similar to that observed in our study. The $\delta^{18}O$ change of −4‰ associated with the $\delta^{13}C$ shift of −7‰ obtained in this study would correspond to a temperature increase of ~ 10–15 °C (using the palaeotemperature equations of Shackleton and Kennett, 1975; Mulitza et al., 2003; Rosales et al., 2004; Waelbroeck et al., 2005). Although the equations were specifically formulated for different types of material (belemnites: Rosales et al., 2004; foraminifers: Rosales et al., 2004; Waelbroeck et al., 2005), they yield surprisingly similar temperatures for our measured carbonate compositions using a theoretical seawater $\delta^{18}O$ value of −1.2‰ (Shackleton and Kennett, 1975). The calculations indicate a temperature change from 13 to 28 °C, with the high temperatures obtained for the low $\delta^{18}O$ and $\delta^{13}C$ samples. A warming of 10–15 °C may appear exaggerated, but rapid (<0.5 Ma in duration) warming of apparently similar magnitude has been documented for the Early Toarcian (Jenkyns, 2003; Bailey et al., 2003; Rosales et al., 2004) and was interpreted as a primary signal. Thus, the fluctuations at the T–J boundary are not unique and are consistent with a model of thermally driven episodic methane release.

Alternatively, cyclic upwelling of anoxic bottom water with ^{12}C-rich dissolved inorganic carbon may also explain the $\delta^{13}C$ fluctuations, but it is difficult to accept as a global phenomenon. Changes in productivity may also release ^{12}C through biomass degradation, but it would have caused long-term changes rather than rapid short-term fluctuations. Massive volcanic CO_2 emission may suddenly change the atmospheric CO_2 level and induce greenhouse warming. However, model simulations suggest that with its average C isotope composition of ~−5‰, massive degassing of mantle-derived CO_2 cannot in itself explain the observed isotopic shifts (Beerling and Berner, 2002).

In summary, episodic dissociation of deep-sea methane hydrate due to rapid temperature rise is the most probable explanation for the observed $\delta^{13}C$ variations and the associated $\delta^{18}O$ changes that are likely, at least partly, to reflect temperature variations.

9.3. Sea-level change across the T–J boundary

Interpretation of sea-level history from the Csővár section is of significance as sea-level changes have been implicated as a factor in the T–J boundary crisis (e.g. Hallam and Wignall, 1999). A sudden regression–transgression couplet at the boundary was claimed to be a factor but supporting evidence has remained controversial. At Csővár, the interpreted relative sea-level curve (Fig. 4) is characterized by a gradual transgressive trend that is punctuated by lowstands associated with third- and fourth-order cycles (Vail et al., 1991; Schlager, 2005). The second observed lowstand, manifest in Bed 30, falls into the Late Rhaetian and correlates with a marked decline in foraminiferan and conodont faunas. Drowning of nearby platforms is indicated by disappearance of typical platform-derived bioclasts. Platform tops were recolonized by crinoids, which commonly occur higher upsection as bioclasts in slope and basinal facies. The local drowning event is tentatively correlated with regional (e.g. in the Northern Calcareous Alps) and global reef crisis at the T–J boundary. Notably, the principal isotope anomaly at Csővár is not correlated with this or any other prominent sea-level change but occurs during the transgressive phase of the next cycle. A similar relationship was observed at the St Audries' Bay section (Hesselbo et al., 2004) and the Lombardian sections (Galli et al., 2005).

The largest relative sea-level fall is recorded by oncoidal facies at 32–34 m, clearly in the Early Hettangian, above the first appearance of Jurassic ammonoids and the distinctive Jurassic radiolarian assemblage.

The observed fourth-order cycles could possibly be controlled by Milankovitch forcing but at present this hypothesis remains untested. The studied interval that spans the Late Rhaetian to Early–Middle Hettangian consists of five cycles. This framework is useful for the observed local sequence of events at the T–J boundary (Fig. 12). The following events took place within a single cycle: (1) disappearance of ephemerally abundant

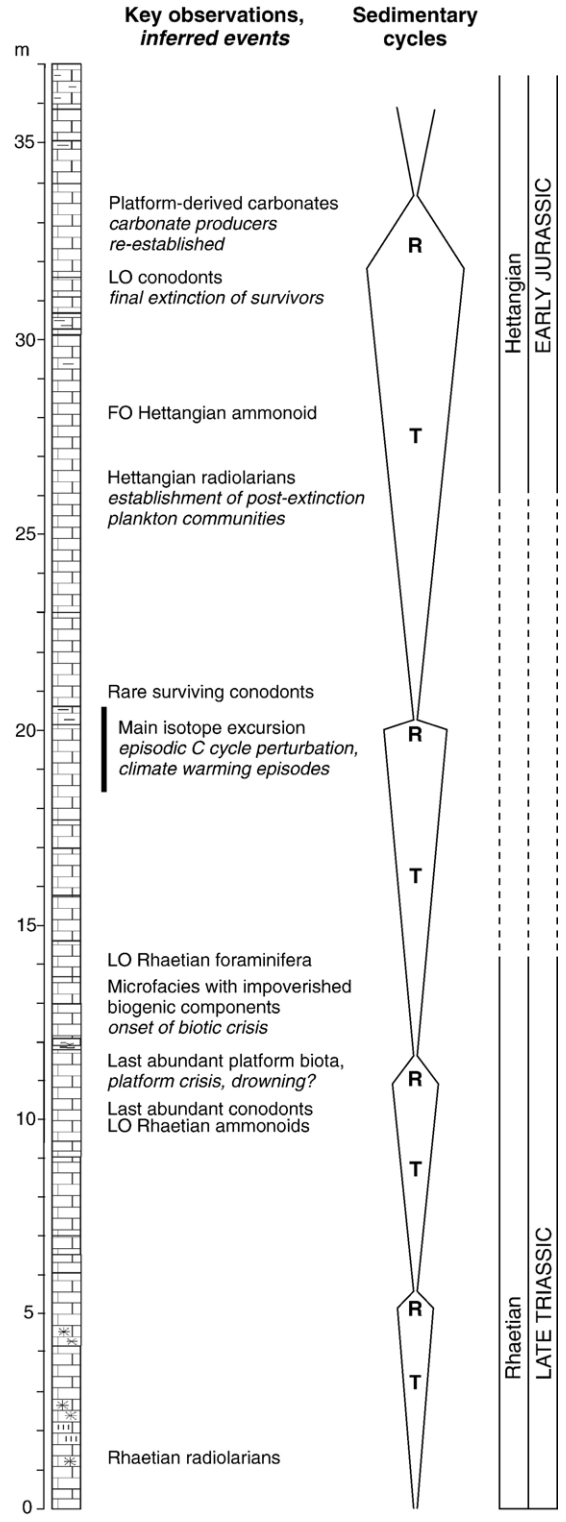

Fig. 12. Summary and chronology of biotic, isotopic, sedimentary and other events observed at the T–J boundary section of Csővár. T—transgressive, R—regressive.

platform-derived biota, possibly related to a drowning event; (2) decline of both planktic and benthic biota (reduction in biogenic sedimentary components, and conodont and foraminiferan diversity); (3) geochemical anomalies in C and O isotopes; and (4) concurrent reduction of TOC. The first appearance of a new, Jurassic radiolarian fauna, the final extinction of decimated conodont populations and recovery of primary production occurred in the following cycle.

10. Conclusions

The Csővár section is an important reference section for the marine T–J boundary in the western Tethys. The T–J boundary is defined by coherent radiolarian, foraminiferan, conodont and ammonoid biostratigraphy. Faunal turnover between the Late Rhaetian *G. tozeri* and the Early Hettangian *C. merum* radiolarian zones is almost complete at the species level. This pattern is similar to the one documented from the margins of Panthalassa.

The succession of *Misikella posthernsteini* and *M. ultima* zones provides a reference for latest Triassic conodont biostratigraphy. Following a pronounced reduction in diversity and abundance, the final extinction of conodonts appears delayed until the termination of sporadic survivors in the earliest Hettangian.

The biotic extinction is reflected in the reduction of both the biogenic components in carbonates and the TOC, the latter thought to represent a productivity crisis followed by a rapid recovery of different producers. However, foraminiferan faunal change is less pronounced and several lineages survive into the Hettangian.

Magnetostratigraphy could not fulfill its potential for independent correlation. All samples that retain primary remanent magnetization are of normal polarity, but an apparent reversed polarity zone at the T–J boundary is proved to result from secondary remagnetization acquired in the Neogene.

The section contains no primary volcanogenic component. There is little change in the clay and heavy mineral composition but elevated heavy mineral content in the lowest Jurassic strata hints at a climatically driven increase of terrigenous influx.

The T–J boundary interval is characterized by a negative $\delta^{13}C$ excursion of as much as −5‰ that is composed of higher frequency fluctuations. Carbon isotope ratios are significantly correlated with $\delta^{18}O$ in two closely spaced parallel sections, after filtering out samples affected by diagenetic alteration. The underlying phenomena are interpreted as episodic perturbations of the global carbon cycle, possibly due to

methane release from gas hydrate dissociation induced by rapid climatic events. Warming in excess of + 10 °C is calculated on the basis of the measured $\delta^{18}O$ values.

An inferred long-term Rhaetian to Hettangian eustatic sea-level rise is superimposed by five short (fourth-order) cycles. The main T–J boundary biotic and isotopic events fall into a single cycle, suggesting that the T–J boundary crisis was potentially a short but not instantaneous event. The sequence and nature of events inferred from the Csővár section are consistent with a scenario of global environmental change and the biotic response triggered by climatic effects of volcanism of the Central Atlantic Magmatic Province.

Acknowledgements

We thank R. Wernli for discussion on foraminifera and H. Kiss help with sample processing. Helpful reviews by A. Coe, S. Hesselbo and G. Price improved the manuscript. Research was supported by the Hungarian Scientific Research Fund (Grants OTKA T042802, T034168, T032260, T037966 and F048341). This is a contribution to IGCP Project 458.

Appendix A. Conodont taxonomic notes (by M. Orchard)

Misikella kovacsi n. sp. (Fig. 6.8)
Derivation of name. In honor of Sándor Kovács (Budapest) who initiated this study of the Csővár conodonts.

Holotype. GSC 120180, from Bed 00/29 (GSC loc. C-305163).
Type locality and stratum. Csővár Limestone Formation, southwestern slope of Vár-hegy at Csővár, Bed 29.

Diagnosis. The P_1 element is a comparatively robust segminate element corresponding to that of other *Misikella* species but characterized by only two denticles above an expanded basal cavity with a V-shaped incision of its posterior margin.

Remarks. This new species is based on a P_1 element that has the same basal characteristics as *M. posthernsteini* and *M. ultima* but which has fewer denticles than both those species. It is likely that its multielement apparatus shares the same ramiform elements as those two species, namely variations on *C. dinodoides* s.f. (= M element) and *N. rhaetica* s.f. (= S_{1-3} elements), with an S_0 element similar to that illustrated in Fig. 6.12.

'*Neohindeodella*' n. sp. A (Fig. 6.25)
Remarks. This element differs from those described by Swift (1989, pl. 37, figs. 5 6, 7 and 8) in bearing four rather than two anterior denticles in front of the cusp, which is identified by its larger size. The anterior process is consequently longer and more downturned, forming a lesser angle with the posterior process, which in this case is incomplete.

?Zieglericonus sp. A (Fig. 6.22)
Remarks. This single element differs from *Z. rhaeticus* in having a cusp that is more upright and turned inward rather than towards the posterior. The "Pa" element illustrated by Swift (1989, pl. 37, fig. 9) from the Langport Member at Normanton Hills appears the same but is more complete at the base. The rare elements may represent another part (P_2?) of the apparatus of *Z. rhaeticus.*

References

Aldridge, R.J., 1988. Extinction and survival in the Conodonta. In: Larwood, G.P. (Ed.), Extinction and Survival in the Fossil Record. Systematics Association Special Volume. Clarendon Press, Oxford, pp. 231–256.

Bagnoli, G., Perri, M.C., Gandin, A., 1985. Ladinian conodont apparatuses from northwestern Sardinia, Italy. Boll. Soc. Palaeontol. Ital. 23, 311–323.

Bailey, T.R., Rosenthal, Y., McArthur, J.M., van de Schootbrugge, B., Thirlwall, M.F., 2003. Paleoceanographic changes of the Late Pliensbachian–Early Toarcian interval: a possible link to the genesis of an Oceanic Anoxic Event. Earth Planet. Sci. Lett. 212, 307–320.

Beerling, D.J., Berner, R.A., 2002. Biogeochemical constraints on the Triassic–Jurassic boundary carbon cycle event. Glob. Biogeochem. Cycles 16 (3) (art. no.-1036).

Benkő, K., Fodor, L., 2002. Csővár környékének szerkezetföldtana (Structural geology near Csővár, Hungary). Földt. Közlöny 132, 223–246.

Bordenave, M.L., Espitalié, J., Leplat, P., Oudin, J.L., Vandenbroucke, M., 1993. Screening techniques for source rock evaluation. In: Bordenave, M.L. (Ed.), Applied Petroleum Geochemistry. Éditions Technip, Paris, pp. 217–276.

Carter, E.S., Hori, R., 2005. Global correlation of the radiolarian faunal change across the Triassic–Jurassic boundary. Can. J. Earth Sci. 42, 777–790.

Carter, E.S., Whalen, P.A., Guex, J., 1998. Biochronology and paleontology of Lower Jurassic (Hettangian and Sinemurian) radiolarians, Queen Charlotte Islands, British Columbia. Geol. Surv. Can. Bull. 496 (162 pp.).

Csontos, L., Vörös, A., 2004. Mesozoic plate tectonic reconstruction of the Carpathian region. Palaeogeogr. Palaeoclimatol. Palaeoecol. 210, 1–56.

Detre, C., Dosztály, L., Hermann, V., 1988. A csővári felső-nóri, sevati fauna (The Upper Norian (Sevatian) fauna of Csővár). A Magyar Állami Földtani Intézet Évi Jelentése az 1986. Évről (Annual Report of the Hungarian Geological Institute, 1986), pp. 53–67.

De Wever, P., Dumitrica, P., Caulet, J.P., Nigrini, C., Caridroit, M., 2001. Radiolarians in the Sedimentary Record. Gordon and Breach Science Publishers, Amsterdam. 533 pp.

Dickens, G.R., 2003. Rethinking the global carbon cycle with a large, dynamic and microbially mediated gas hydrate capacitor. Earth and Planet. Sci. Lett. 213, 169–183.

Dickens, G.R., O'Neil, J.R., Rea, D.K., Owen, R.M., 1995. Dissociation of oceanic methane hydrate as a cause of the carbon isotope excursion at the end of the Paleocene. Paleoceanography 10, 965–971.

Espitalié, J., Deroo, G., Marquis, F., 1986. La pyrolyse Rock-Eval et ses applications. Revue de L'Institute Francais du Petrole, vol. 40/5. Éditions Technip, Paris, pp. 563–784.

Galli, M.T., Jadoul, F., Bernasconi, S.M., Weissert, H., 2005. Anomalies in global carbon cycling and extinction at the Triassic/Jurassic boundary: evidence from a marine C-isotope record. Palaeogeogr. Palaeoclimatol. Palaeoecol. 216, 203–214.

Gawlick, H.-J., Frisch, W., Vecsei, A., Steiger, T., Böhm, F., 1999. The change from rifting to thrusting in the Northern Calcareous Alps as recorded in Jurassic sediments. Geol. Rundsch. 87, 644–657.

Guex, J., Bartolini, A., Atudorei, V., Taylor, D., 2004. High-resolution ammonite and carbon isotope stratigraphy across the Triassic–Jurassic boundary at New York Canyon (Nevada). Earth Planet. Sci. Lett. 225, 29–41.

Haas, J., 2002. Origin and evolution of Late Triassic backplatform and intraplatform basins in the Transdanubian Range, Hungary. Geol. Carpath. 53, 159–178.

Haas, J., Tardy-Filácz, E., 2004. Facies changes in the Triassic–Jurassic boundary interval in an intraplatform basin succession at Csővár (Transdanubian Range, Hungary). Sediment. Geol. 168, 19–48.

Haas, J., Kovács, S., Krystyn, L., Lein, R., 1995. Significance of Late Permian–Triassic facies zones in terrane reconstructions in the Alpine North Pannonian domain. Tectonophysics 242, 19–40.

Haas, J., Tardy-Filácz, E., Oravecz-Scheffer, A., Góczán, F., Dosztály, L., 1997. Stratigraphy and sedimentology of an Upper Triassic toe-of-slope and basin succession at Csővár, Hungary. Acta Geol. Hung. 40, 111–177.

Hallam, A., 1990. The end-Triassic mass extinction event. In: Sharpton, V.L., Ward, P.D. (Eds.), Global Catastrophes in Earth History; An Interdisciplinary Conference on Impacts, Volcanism, and Mass Mortality. Geol. Soc. Am., Spec. Pap., vol. 247, pp. 577–583.

Hallam, A., 2002. How catastrophic was the end-Triassic mass extinction? Lethaia 35, 147–157.

Hallam, A., Wignall, P.B., 1999. Mass extinctions and sea-level changes. Earth-Sci. Rev. 48, 217–250.

Hedges, J.I., Keil, R.G., 1995. Sedimentary organic-matter preservation —an assessment and speculative synthesis. Mar. Chem. 49, 81–115.

Hesselbo, S.P., Gröcke, D.R., Jenkyns, H.C., Bjerrum, C.J., Farrimond, P., Morgans Bell, H.S., Green, O.R., 2000. Massive dissociation of gas hydrate during a Jurassic oceanic anoxic event. Nature 406, 392–395.

Hesselbo, S.P., Robinson, S.A., Surlyk, F., Piasecki, S., 2002. Terrestrial and marine mass extinction at the Triassic–Jurassic boundary synchronized with major carbon-cycle perturbation: a link to initiation of massive volcanism? Geology 30, 251–254.

Hesselbo, S.P., Robinson, S.A., Surlyk, F., 2004. Sea-level change and facies development across potential Triassic–Jurassic boundary horizons, SW Britain. J. Geol. Soc. (Lond.) 161, 365–379.

Hounslow, M.W., Posen, P.E., Warrington, G., 2004. Magnetostratigraphy and biostratigraphy of the Upper Triassic and lowermost Jurassic succession, St. Audrie's Bay, UK. Palaeogeogr. Palaeoclimatol. Palaeoecol. 213, 331–358.

Jenkyns, H.C., 2003. Evidence for rapid climate change in the Mesozoic–Palaeogene greenhouse world. Philos. Trans. R. Soc. Lond. Ser. A: Math. Phys. Sci. 361, 1885–1916.

Kennett, J.P., Cannariato, K.G., Hendy, I.L., Behl, R.J., 2000. Carbon isotopic evidence for methane hydrate instability during Quaternary interstadials. Science 288, 128–133.

Kent, D.V., Olsen, P.E., Witte, W.K., 1995. Late Triassic–earliest Jurassic geomagnetic polarity sequence and paleolatitudes from drill cores in the Newark Rift Basin, eastern North America. J. Geophys. Res. 100 (B8), 14,965–14,998.

Koike, T., 1994. Skeletal apparatus and its evolutionary trends in a Triassic conodont *Ellisonia dinodoides* (Tatge) from the Taho Limestione, southwestern Japan. Trans. Proc. Pal. Soc. Jpn., New Series, vol. 173, pp. 366–383.

Kovács, S., Szederkényi, T., Haas, J., Buda, G., Császár, G., Nagymarosy, A., 2000. Tectonostratigraphic terranes in the pre-Neogene basement of the Hungarian part of the Pannonian area. Acta Geol. Hung. 43, 225–328.

Kozur, H., 1993. First evidence of Liassic in the vicinity of Csővár (Hungary), and its palaeogeographic and palaeotectonic significance. Jahrb. Geol. Bundesanst. 136, 89–98.

Kozur, H., Mostler, H., 1990. Saturnaliacae Deflandre and some other stratigraphically important Radiolaria from the Hettangian of Lenggries/Isar (Bavaria/Northern Calcareous Alps). Geol. Paläntol. Mitt. 17, 179–248.

Kozur, H., Mock, R., 1991. New Middle Carnian and Rhaetian conodonts from Hungary and the Alps. Stratigraphic importance and tectonic implications for the Buda Mountains and adjacent areas. Jahrb. Geol. Bundesanst. 134, 271–297.

Lakew, T., 1990. Microfacies and cyclic sedimentation of the Upper Triassic (Rhaetian) Zu Limestone (Southern Alps). Facies 22, 187–232.

Márton, E., 1998. The bending model of the Transdanubian Central Range (Hungary) in the light of Triassic palaeomagnetic data. Geophys. J. Int. 134, 625–633.

Márton, E., Pécskay, Z., 1998. Complex evaluation of K/Ar isotope data of the Miocene ignimbritic volcanics in the Bükk Foreland, Hungary. Acta Geol. Hung. 41, 467–476.

Marzoli, A., Renne, P.R., Piccirillo, E.M., Ernesto, M., Bellieni, G., De Min, A., 1999. Extensive 200-million-year-old continental flood basalts of the Central Atlantic Magmatic Province. Science 284, 616–618.

Marzoli, A., Bertrand, H., Knight, K.B., Cirilli, S., Buratti, N., Verati, C., Nomade, S., Renne, P.R., Youbi, N., Martini, R., Allenbach, K., Neuwerth, R., Rapaille, C., Zaninetti, L., Bellieni, G., 2004. Synchrony of the Central Atlantic magmatic province and the Triassic–Jurassic boundary climatic and biotic crisis. Geology 32, 973–976.

Mulitza, S., Boltovskoy, D., Donner, B., Meggers, H., Paul, A., Wefer, G., 2003. Temperature: $\delta^{18}O$ relationships of planktonic foraminifera collected from surface waters. Palaeogeogr. Palaeoclimatol. Palaeoecol. 202, 143–152.

McCrea, J.M., 1950. On the isotopic chemistry of carbonates and a paleotemperature scale. J. Chem. Phys. 18, 849–857.

Olsen, P.E., Kent, D.V., Sues, H.-D., Koeberl, C., Huber, H., Montanari, A., Rainforth, E.C., Fowell, S.J., Szajna, M.J., Hartline, B.W., 2002. Ascent of dinosaurs linked to an iridium anomaly at the Triassic–Jurassic boundary. Science 296, 1305–1307.

Orchard, M.J., 2005. Multielement conodont apparatuses of Triassic Gondolelloidea. Spec. Pap. Palaeontol. 73, 1–29.

Pálfy, J., 2003. Volcanism of the Central Atlantic Magmatic Province as a potential driving force in the end-Triassic mass extinction. In: Hames, W.E., McHone, J.G., Renne, P.R., Ruppel, C. (Eds.), The Central Atlantic Magmatic Province: Insights from Fragments of Pangea. AGU Geophys. Mono. Ser., vol. 136, pp. 255–267.

Pálfy, J., Dosztály, L., 2000. A new marine Triassic–Jurassic boundary section in Hungary: preliminary results. In: Hall, R.L., Smith, P.L. (Eds.), Advances in Jurassic Research 2000. GeoResearch Forum, vol. 6. TransTech Publications, Zurich, pp. 173–179.

Pálfy, J., Mortensen, J.K., Carter, E.S., Smith, P.L., Friedman, R.M., Tipper, H.W., 2000. Timing the end-Triassic mass extinction: first on land, then in the sea? Geology 28, 39–42.

Pálfy, J., Demény, A., Haas, J., Hetényi, M., Orchard, M., Vető, I., 2001. Carbon isotope anomaly and other geochemical changes at the Triassic–Jurassic boundary from a marine section in Hungary. Geology 29, 1047–1050.

Pessagno, E., Blome, C.D., Carter, E.S., Macleod, N., Whalen, P.A., Yeh, K.-Y., 1987. Preliminary radiolarian zonation for the Jurassic of North America, Studies of North American Jurassic Radiolaria, Part 2. Cushman Lab. Foraminifer. Res. Spec. Publ. 23, 1–18.

Reynolds Jr., R.C., Hower, J., 1970. The nature of interlaying in mixed-layer illite-montmorillonite. Clays Clay Miner. 18, 25–36.

Rosales, I., Quesada, S., Robles, S., 2004. Palaeotemperature variations of Early Jurassic seawater recorded in geochemical trends of belemnites from the Basque-Cantabrian Basin, northern Spain. Palaeogeogr. Palaeoclimatol. Palaeoecol. 203, 253–275.

Salmon, V., Derenne, S., Largeau, C., Lallier-Vergs, E., Beaudoin, B., Bardoux, G., Mariotti, A., 1997. First indication of a major role for the sorptive protection pathway in kerogen formation (Cenomanian black shale, central Italy). 18th International Meeting on Organic Geochemistry, Maastricht, Abstract Volume, pp. 849–850.

Schlager, W., 2005. Carbonate Sedimentology and Sequence Stratigraphy. Concepts in Sedimentology and Paleontology, vol. 8. SEPM, Tulsa, OK. 200 pp.

Sepkoski Jr., J.J., 1996. Patterns of Phanerozoic extinction: a perspective from global data bases. In: Walliser, O.H. (Ed.), Global Events and Event Stratigraphy in the Phanerozoic. Springer, Berlin, pp. 35–51.

Shackleton, N.J., Kennett, J.P., 1975. Paleotemperature history of the Cenozoic and the initiation of Antarctic glaciation: oxygen and carbon isotope analyses in DSDP sites 277, 279 and 281. In: Kennett, J.P. (Ed.), Initial Reports of the Deep Sea Drilling Project, vol. 29. United States Government Printing Office, pp. 743–755.

Spence, G.H., Tucker, M.E., 1997. Genesis of limestone megabreccias and their significance in carbonate sequence stratigraphic models: a review. Sediment. Geol. 112, 163–193.

Stathoplos, L., Hare, P.E., 1993. Bleach removes labile amino acids from deep sea planktonic foraminiferal shells. J. Foraminiferal Res. 23, 102–107.

Swift, A., 1989. First records of conodonts from the Late Triassic of Britain. Palaeontology 32, 325–333.

Szabó, J., 1860. Geologische Detailkonte des Grenzgebietes des Nograder und Pesther Comitates. Jahrbuch des Kaiserlich-Königlichen Geologischen Reichanstalt, Sitzungberichte (Sitzung am 10. Jänner 1860), pp. 41–44.

Tanner, L.H., Lucas, S.G., Chapman, M.G., 2004. Assessing the record and causes of Late Triassic extinctions. Earth-Sci. Rev. 65, 103–139.

Vadász, E., 1910. A Duna-balparti idősebb rögök őslénytani és földtani viszonyai [Palaeontology and geology of older blocks on the left side of Danube]. Magy. Királyi Földt. Intéz. Évkv. [Annals of the Royal Hungarian Geological Institute] 18, 101–171.

Vail, P.R., Audemard, F., Bowman, S.A., Eisner, P.N., Perez-Cruz, C., 1991. The stratigraphic signatures of tectonics, eustasy and sedimentology—an overview. In: Einsele, G., Ricken, W., Seilacher, A. (Eds.), Cycles and Events in Stratigraphy. Springer, Berlin, pp. 617–659.

Waelbroeck, C., Mulitza, S., Spero, H., Dokken, T., Kiefer, T., Cortijo, E., 2005. A global compilation of Late Holocene planktonic foraminiferal $\delta^{18}O$: relationship between surface water temperature and $\delta^{18}O$. Quat. Sci. Rev. 24, 853–868.

Ward, P.D., Haggart, J.W., Carter, E.S., Wilbur, D., Tipper, H.W., Evans, T., 2001. Sudden productivity collapse associated with the Triassic–Jurassic boundary mass extinction. Science 292, 1148–1151.

Ward, P.D., Garrison, G.H., Haggart, J.W., Kring, D.A., Beattie, M.J., 2004. Isotopic evidence bearing on Late Triassic extinction events, Queen Charlotte Islands, British Columbia, and implications for the duration and cause of the Triassic/Jurassic mass extinction. Earth Planet. Sci. Lett. 224, 589–600.